STUDY PERFORMANCE OF A THREE-PHASE INDUCTION MOTOR UNDER UNBALANCED CONDITIONS

by

IBRAHIM ABDOU IBRAHIMA (170021172)

ABDOURRAHMAN OMAR ABDOU (170021173)

MOHAMAN DJIBRILLA (170021180)

A Thesis Submitted to the Academic Faculty in Partial Fulfillment of the Requirements for the Degree of

BACHELOR OF SCIENCE IN ELECTRICAL AND ELECTRONIC ENGINEERING

Department of Electrical and Electronic Engineering

Islamic University of Technology (IUT)

Gazipur, Bangladesh

May 2022

STUDY PERFORMANCE OF A THREE-PHASE INDUCTION MOTOR UNDER UNBALANCED CONDITIONS

Approved by:

Dr. MD. FOKHRUL ISLAM

Supervisor and Professor,

Department of Electrical and Electronic Engineering,

Islamic University of Technology (IUT),

Board Bazar, Gazipur-1704.

Date: ……

Declaration of Authorship

This is the attestation of the work done in the thesis paper by the students Ibrahim Abdou Ibrahima, Abdurrahman Omar Abdou, and Mohaman Djibrilla under the supervision of Dr. Md. Fokhrul Islam, Professor of Department of Electrical and Electronic Engineering (EEE), Islamic University of Technology (IUT), a subsidiary organ of the Organization of Islamic Cooperation (OIC).

Authors

_____

IBRAHIM ABDOU IBRAHIMA

ID-170021172

_____

ABDOURRAHMAN OMAR ABDOU

ID-170021173

_____

MOHAMAN DJIBRILLA

ID-170021180

Table of Contents

Acknowledgments

First and foremost, praise and glory to ALLAH, the Almighty for giving us the capability to pursue this study up this level.

It is a pleasure to acknowledge the assistance received from several people during the preparation of this thesis work. We greatly appreciate the help from our supervisor Professor Dr. Md. Fokhrul Islam, gave us his precious time and attention in order for us to be able to achieve our goal. We also thank all those who contributed to our success.

Finally, we would like to thank our family members for their support and continuous encouragement in the completion of this thesis.

Abstract

The aim of this research is to investigate and illustrate the impact of unbalanced supply voltages on the operation and performance of a three-phase induction motor. Three-phase supply voltages, unlike single-phase supply voltages, can become unbalanced in a variety of ways, whereas a balanced situation maintains consistent voltage magnitude and angles in all three phases, albeit a truly balanced condition is impossible to achieve in practice. Imbalance situations might arise on several ranges and it can be harmful to the motor. A 3 phase induction machine is designed to work under balanced conditions, but under unbalanced situations, it can experience a variety of complex changes in its mechanical and electrical variables. This study analyzes distinct symmetrical and asymmetrical settings in terms of mechanical and electrical responses to better understand the magnitude of such changes. Rotor and stator currents, electromechanical torque, and rotor speed are among the reactions. To investigate these responses and motor behavior under various unbalanced conditions, a simulation model of a three-phase induction machine is employed, along with various software-generated subsystems. The motor's final throughput is calculated using torque-speed characteristics and derating factor curves for various unbalanced voltage circumstances. A common view is that a complete breakdown of a phase is far more harmful to motor function than a percentage increase or decrease in voltage level or phase. Furthermore, a change in the phase angle of the voltage has indeed been observed to cause more changes in the responses than a change in the voltage magnitude. The quantifiable correlation between voltage imbalance and the resultant mechanical and electrical outputs will aid in the design of proper voltage imbalance prevention. This research would also aid in the development of derating factors for motors running in various imbalanced circumstances.

List of Figures

List of Tables

Chapter 1 : Introduction

Because of their durability, efficiency, reliability, and low operating costs, three-phase induction motors (3P-IM) are widely utilized in industrial applications. While single-phase induction motors are more popular in domestic and light industrial applications, three-phase induction motors are used in light to heavy industrial uses. Conveyors, pumps, ventilation, compressors, and many other drive applications in the manufacturing and processing industries are powered by 3P-IMs.

Because the frequency of the electrical power source determines the induction motor's speed, it has been successfully used in applications where a constant speed is required. They are more popular than their rival DC motor drives, which are often employed in variable speed applications, due to their lower cost and better power output. Induction motor speeds may now be adjusted by changing the AC current frequency thanks to controlling electronics [1]. Variable speed drives have become more efficient and cost-effective as a result of this advancement, and induction motors have largely supplanted DC motors in most industrial applications. 3P-IMs consume almost 75% of all industrial electricity [2]. 3P-IMs are used in about 80% of commercial applications [3]. Greater economy and performance can result in significant savings in industrial applications, considering the massive quantity of power utilized by these motors. The quality and reliability of the electric power system that energizes the motor determine the motor's performance and throughput. Because electrical power networks are made up of a complex network of generation, transmission, distribution, and use, faults and imbalances can occur at any moment and in varying degrees of size and duration, affecting the overall quality of the electrical power delivered. The majority of current electric machines include built-in safeguards to prevent damage from poor power quality. Long-term exposure to a poor electric power source, on the other hand, may result in subtle losses or harm to the machine's performance and lifespan. In industries, even a tiny percentage reduction in efficiency can result in a considerable total loss of mechanical output and production loss. As a result, the influence of electrical input imbalance of power on AC machines is an important research topic. Such research evaluates both the loss of performance and the design of preventative measures to compensate for or prevent such losses.

Despite its multiple benefits and applications, 3P-IMs have a number of limitations, one of which is their vulnerability to unbalanced voltage circumstances. Unbalanced voltage might manifest itself as either a magnitude discrepancy or as phase asymmetries. Under unbalanced

situations, the motor is subjected to a simultaneous supply of over and under voltages across many lines. [4]. On various scales, these events diminish the performance of the 3P-IM. An unbalanced supply situation can be introduced by a failure in a transmission line or an unequal distribution of single-phase loads. An abrupt change in loads, such as the shutdown of a plant, unbalanced line or phase impedances in the power system, or an open delta transformer connection, can also cause the supply voltage to become unbalanced. According to an ANSI assessment, approximately 32% of the whole electrical system in the United States has imbalanced levels ranging from 1% to 3% [3]. Voltage imbalances should not exceed 2%, according to IEC guidelines [3, 5]. However, due to the complexity of the loads and their distribution systems, it is impossible to have a power system that is completely devoid of any type of imbalance. Depending on their severity and characteristics, these unbalanced circumstances have varying effects on the system [6]. To assess their effect on mechanical throughput and economy, the performance of a 3P-IM must be thoroughly examined under various unbalanced scenarios.

I. Objectives

Computer-based simulations were used in this study to look at the impact of four different situations on the 3P-IM characteristics and performance. These four situations, which cause imbalanced voltage, are widely classified as follows:

➢ Phase loss in a three-phase supply;
➢ Unbalanced magnitudes in the three-phase supply voltage;
➢ Unbalanced phase angles in the three-phase supply voltage;
➢ In the three-phase supply voltage, both unbalanced magnitudes and phase angles exist.

It is expected that this work may spark additional research utilizing comparable software simulations. Software simulation could be used to simulate real-world circumstances at little or low cost, eliminating the need for substantial and costly underlying hardware and setup. An experimental investigation may necessitate the manipulation of a large number of factors and variables, which may be impossible in a real-world hardware setup. Moreover, in energy systems, rendering events such as faults or unbalanced conditions can be dangerous and harmful to the unit under test if suitable protection measures are not included. Simulations

have been used in a variety of research relating to power systems and machinery [7]. The impact of loading an induction motor during an imbalanced voltage event was demonstrated by *Jayatunga et al*. in a simulation [8]. A simulation can give you a good idea of what might happen in real life, and it might even help you with induction motor design.

II.   Literature Review

Raj et al. investigated the supply voltage distortion's effect on the performance of a 5 HP 3P-IM [9]. The analysis shows that an imbalanced but undistorted voltage exists waveforms have a worse effect on 3P-IMs than balanced but distorted (non-sinusoidal) waveforms. The distortion of non-sinusoidal supply voltages results in the formation of damaging harmonics, which degrade motor performance by adding pulsing torque and noise [9]. Unbalanced voltages cause a loss of efficiency due to counteracting torque, which cancels out mechanical throughput or torque, according to *Williams* [10]. Several investigations have found that induction motors overheat and fail prematurely owing to unbalanced currents [5], [11]. According to a report from the US Department of Energy, a 10° C increase in temperature beyond typical operating temperature can cut the lifespan of a 3P-IM in half [12].

Unbalanced voltages have been shown to have the following impacts on 3P-IMs in a number of contemporaneous experiments [9], [13], and [14]. To begin, the entire output torque, which really is effectively the motor's throughput, decreases [13]. Moreover, it reduces efficiency [10], as well as power factor [15]. Third, vibration and noise [6, 16], as well as rotor rising temperatures, can cause wear and aging, affecting steady-state operating parameters. Lastly, a decrease in efficiency might cause significant financial loss [17].

The research examines several mechanical and electrical characteristics of a 3P-IM under these imbalanced voltage conditions in order to better understand the associated consequences of each operating situation. The impacts must be described by contrasting the parameters of 3P-IMs that are exposed to both symmetrical and asymmetrical conditions. To enable such analysis, the performance of a 3P-IM is also modeled under usual circumstances.

III.   Requirements for this Research

This study's experimentation is separated into two components. The electrical properties of the 3P-IM under test, such as reactance and resistance values, are measured in the first stage. In the lab, three tests are performed on an actual 3P-IM, including blocked-rotor, no-load, and DC testing. These tests are carried out to determine all of the electrical parameters needed for the simulation in the following section of the research. The stator resistance is determined by the DC test, whereas the stator reactance, but also the rotor resistance and reactance, are determined by the blocked-rotor test. The magnetizing reactance is determined by the no-load test. The tests are carried out in order, with the results from one test being applied to the next. All of the test scenarios for unbalanced voltages are displayed and simulated in software in the second phase of the study. The parameter values collected in the first part are utilized to build a 3P-IM software model. The 3P-IM model is used to simulate and compare various variables and results when subjected to various unbalanced voltage scenarios. Certain features are required of the simulation application, such as the ability to produce displays and plot various specified variables such as output current, speed, and torque. These variables and charts are used to demonstrate and compare the effects of balanced and unbalanced voltage scenarios on the 3P-IM. The induction motor's rating specifications are necessary to establish the physical parameters and are employed in various computational phases throughout the simulation. These requirements, as indicated in Table 1, are provided by the vendor and remain constant for the duration of the experiment. The model is based on a Toshiba 0.37kW three-phase motor and employs a squirrel-caged rotor 3P-IM in a wye configuration.

The variables are translated to a simpler reference frame to enable the analysis of three-phase values in the simulation. Otherwise, due to the presence of time-varying inductances, the equations for determining the performance of a 3P-IM are time-consuming to derive and apply. To eliminate time-dependent inductance in the performance equations, an alternative technique known as the Park's transformation is used. The Park's transformation converts the usual *abc* reference frame to a *dq0* reference frame, removing time-dependent inductances from the performance calculations. In this study, the *dq0* reference frame is used since it simplifies the analysis.

Table 1 : characteristics of the experimental Induction machine

Parameters	Values
Power	0.37kW
Frequency	50Hz
Rotor Speed	1410 rpm
Number of poles	4
Phase	3
Connection type	Wye (Y)
Rated Voltage	415 V
Rated Current	1.1 A

Chapter 2 : Overview

The squirrel cage motor is the most popular 3P-IM design and is more extensively used than wrapped rotor motors. This is due to the fact that the wound rotor type necessitates more maintenance and wear due to its associated brushes and slide rings. Induction motors can use both wye and delta-linked stator windings.

I.   Stator

Because the stator is the motor's external component, the windings in it may be seen from the outside. The stator windings of a 3P-IM are constructed differently than in a single-phase or another polyphase motor. The stator part is made up of a laminated iron core with slots for the winding coils to be woven into. Because they are designed and function 120° out of phase, the three stator windings overlap. The stator windings have low resistance and are insulated between them with varnish or an oxide-type coating [18].

II.   Rotor

A squirrel-cage rotor has a fixed shaft that houses a laminated iron core, bearings, and rotor conductors. Parallel slots are carved into the cylindrical laminated core to accommodate the rotor conductors. Where the rotor bars are fitted into the laminated iron core, thick bars are employed as rotor conductors rather than wires. These rotor bars' ends are short-circuited with the assistance of two solid rings. This design aids in preventing external resistance from developing in series with the rotor. Copper strips soldered to copper rings are commonly used in the construction of these. The materials most typically utilized to produce the rotors of small and medium-sized motors are aluminum and specific metal alloys. To provide electrical continuity, the end rings are either welded or attached to the rotor.

The motor's performance is also affected by the electrical parameters and rotor bar characteristics. The reactance will grow with deeper bars in the rotor structure. This creates a smaller pull-out torque and a weaker beginning current. The rotor conducting bars are oriented asymmetrically in relation to the motor shaft. These locations produce a smooth, consistent acceleration upon motor startup.

III.   Three-phase induction motor operation

Each of the three 120° split-phase stator windings gets alternating current. This current flowing through the stator windings generates a magnetic field that rotates at the synchronous speed, N_s. The value of N_s is determined by the motor's design. N_s is calculated by the number of poles P in the motor for a certain frequency f_{se} of the supplied electric

Synchronous speed is defined as:

$$Ns = \frac{120 * fse}{P} \qquad\qquad (1)$$

Where:

N_s is in revolution per minute (rev/min)

f_{se} in Hertz (Hz)

P is the pole number of the motor

The *rotating magnetic flux* (RMF) created by the rotation throughout the air gap is reduced by the short-circuited rotor bars. The induced voltage pushes a current through the rotor bars, creating a magnetic field. The magnetic field created in the rotor interacts with the magnetic field in the stator to produce torque, which causes the rotor to revolve. The magnetic field's torque changes according to the rotor current and flux density. In essence, the magnetic fields of the stator and rotor revolve at the same synchronous speed. The magnetic field of the rotor constantly rotates at the same speed. However, the rotor speed is somewhat slower than the synchronous speed [21].

The *slip* (S) is the difference between the rotor and synchronous speeds (N_s & N_r). When a mechanical load is applied to the shaft, the rotor slows down, resulting in increased slip, which directly influences the rotor's torque. Eq. 2 describes slip speed (N_{slip}).

$$Nslip = N_s - N_r$$
$$\omega slip = \omega s - \omega r \qquad\qquad (2)$$

Where:

N_s is the synchronous speed (in rev/min)

N_r and ωr mechanical speed of the machine

ωs is the angular velocity (rad/sec)

The ratio between the slip speed and the synchronous speed is called the slip of the induction machine.

$$S = \frac{Ns - Nr}{Ns} \tag{3}$$

It is obvious that when the slip approaches zero, the motor works closer to synchronous speed, and as the slip reaches one, the rotor stops. The rotor frequency may be calculated using the definitions of slip and frequency of the power source.

$$fre = Sfse \tag{4}$$

$$= \frac{P}{120}(Ns - Nr) \tag{5}$$

An induction motor's performance may be assessed using its equivalent circuit diagram. It is employed in this study to determine the equations relating to the induction motor's power and torque. The per-phase equivalent circuit of a 3P-IM is shown in Figure 1.
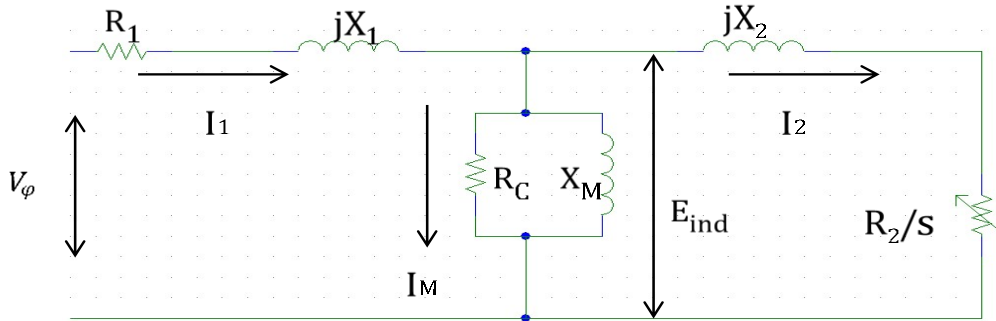
Figure 1 : Circuit diagram induction motor (equivalent single phase)

I_1: stator current;

V_φ: Voltage per phase;

X_M: Magnetizing inductance;

E_{ind}: Induced Voltage (rotor side);

R_1: Stator resistance (per phase);

$R2$: Rotor resistance (per phase);

X_1 and X_2: Respectively Stator and Rotor leakage reactance per phase.

The per-phase input current may be computed using Figure 1.

$$I_1 = \frac{V\varphi}{Zeq} \tag{6}$$

Z_{eq} is the per phase impedance of the three-phase induction machine.

The phase voltage, line current, and power factor are used to calculate the input power P_{in} of a three-phase induction motor.

$$P_{in} = 3V\varphi I1cos\theta \qquad (7)$$

The mechanical output power (P_{out}) is determined by the load torque T_L and the rotational velocity ω_m.

$$P_{out} = T_L\omega_m \qquad (8)$$

Induced Torque $\qquad T_{ind} = \dfrac{Pconv}{\omega m} = \dfrac{PAG}{\omega s} \qquad (9)$

Where, P_{conv} is the converted power and P_{AG} is the air gap power.

P_{AG} can be expressed as:

$$P_{AG} = P_{in} - P_{scl} - P_{core}$$

$$P_{AG} = 3I^2{}_2 * \frac{R2}{S} \qquad (10)$$

Again where we have: P_{scl}, P_{core} are respectively stator copper and core loss.

The associated equations in Figure 2 [18] depict the conversion of input electrical energy to output mechanical power as well as internal losses.
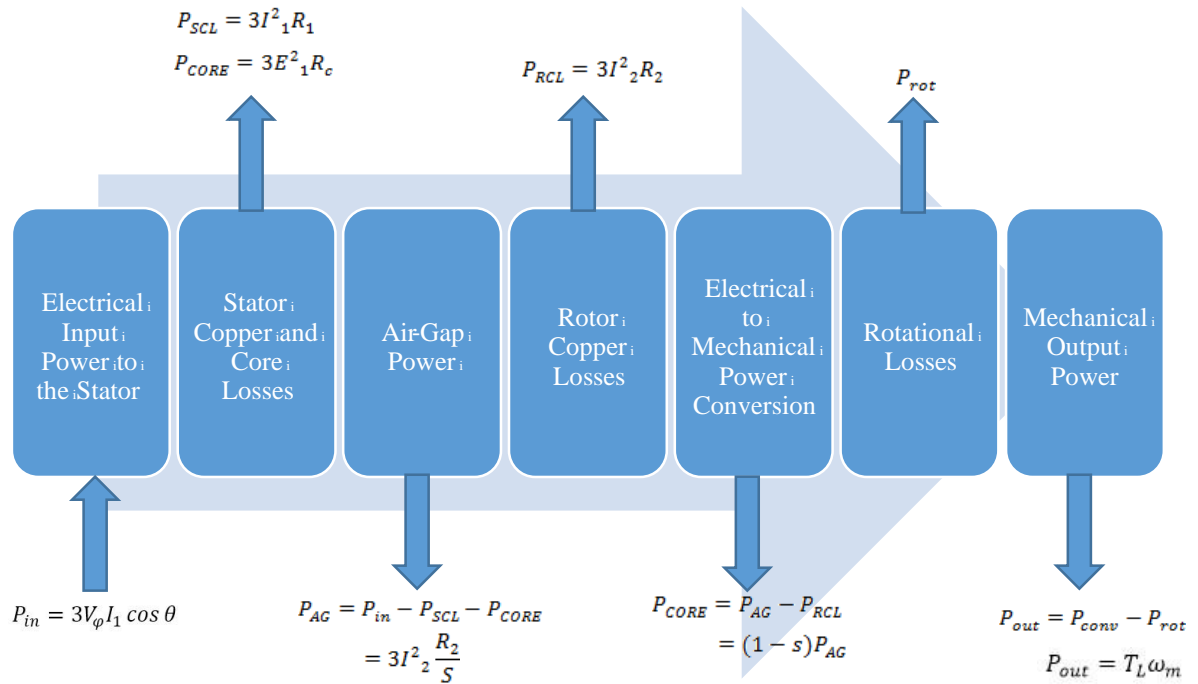

Figure 2 : Power flow diagram 3IM

The voltage equations for a 3P-IM can only be calculated by utilizing the input current and internal impedances. However, these voltages are also a function of the magnetic flux connections with respect to time, which complicates the calculations even further. The input

voltages across each of the three phases of the stator terminals may be represented by the following equations [22]:

$$V_{as} = r2ias + \frac{d\lambda as}{dt}$$

$$V_{bs} = r2ibs + \frac{d\lambda bs}{dt} \qquad (11)$$

$$V_{cs} = r2ics + \frac{d\lambda cs}{dt}$$

The three-phase rotor voltages are magnetically driven by the stator flux linkage and may be described by Eq. 12 [22]:

$$V_{ar} = r2iar + \frac{d\lambda ar}{dt}$$

$$V_{br} = r2ibr + \frac{d\lambda br}{dt} \qquad (12)$$

$$V_{cr} = r2icr + \frac{d\lambda cr}{dt}$$

The variables r, V, I, and in Eq. 11-12 represent resistance, voltage, current, and flux linkage values. Subscripts a, b, and c represent the three-phase values, whereas subscripts s and r represent the stator and rotor, respectively. The mutual inductances and line currents of the stator and rotor can be used to calculate different flux linkages in the following equations. These flow connections are presented in Eq.13, using the formulas supplied by Krause [22]:

$$\lambda_{as} = L_{asas}i_{as} + L_{asbs}i_{bs} + L_{ascs}i_{cs} + L_{asar}i_{ar} + L_{asbr}i_{br} + L_{ascr}i_{cr}$$

$$\lambda_{bs} = L_{bsbs}i_{as} + L_{bsbs}i_{bs} + L_{bscs}i_{cs} + L_{bsbr}i_{br} + L_{bsbr}i_{br} + L_{bscr}i_{cr}$$

$$\lambda_{cs} = L_{cscs}i_{cs} + L_{csbs}i_{bs} + L_{cscs}i_{cs} + L_{cscr}i_{cr} + L_{csbr}i_{br} + L_{cscr}i_{cr} \qquad (13)$$

$$\lambda_{ar} = L_{aras}i_{as} + L_{arbs}i_{bs} + L_{arcs}i_{cs} + L_{arar}i_{ar} + L_{arbr}i_{br} + L_{arcr}i_{cr}$$

$$\lambda_{br} = L_{bras}i_{as} + L_{brbs}i_{bs} + L_{brcs}i_{cs} + L_{brar}i_{ar} + L_{brbr}i_{br} + L_{brcr}i_{cr}$$

$$\lambda_{cr} = L_{cras}i_{as} + L_{crbs}i_{bs} + L_{crcs}i_{cs} + L_{crar}i_{ar} + L_{crbr}i_{br} + L_{crcr}i_{cr}$$

In the preceding equations, indicates the inductance, while the other variables and subscripts relate to the previously indicated values. For example, indicates the inductance between the rotor on phase b and the stator on phase a. The stator self-inductance at each phase a, b, or c is equal where $L_{asas} = L_{asbs} = L_{ascs} = Li_s + L_{ms} * Li_s$ is the leakage inductance of the stator, and the magnetizing inductance is computed using the equation:

$$L_{ms} = (\frac{Ns}{2})^2 * \frac{\mu 0 r l N s 2\pi}{4g} \qquad (14)$$

where r and l are the rotor cylinder's radius and length, respectively, and g is the length of the air gap. Equations (15-17) may be used to express the motor's winding inductances in matrix form:

$$
Ls = \begin{pmatrix}
Lls + Lms & \frac{-1}{2}Lms & \frac{-1}{2}Lms \\
\frac{-1}{2}Lms & Lls + Lms & \frac{-1}{2}Lms \\
\frac{-1}{2}Lms & \frac{-1}{2}Lms & Lls + Lms
\end{pmatrix}
\tag{15}
$$

$$
Lr = \begin{pmatrix}
Llr + Lmr & \frac{-1}{2}Lmr & \frac{-1}{2}Lmr \\
\frac{-1}{2}Lmr & Llr + Lmr & \frac{-1}{2}Lmr \\
\frac{-1}{2}Lmr & \frac{-1}{2}Lmr & Llr + Lmr
\end{pmatrix}
\tag{16}
$$

$$
Lsr = \begin{pmatrix}
cos\theta r & \cos(\theta r + \frac{2\pi}{3}) & \cos(\theta r - \frac{2\pi}{3}) \\
\cos(\theta r - \frac{2\pi}{3}) & cos\theta r & \cos(\theta r + \frac{2\pi}{3}) \\
\cos(\theta r + \frac{2\pi}{3}) & \cos(\theta r - \frac{2\pi}{3}) & cos\theta r
\end{pmatrix}
\tag{17}
$$

The terms L_r, L_s, and L_{sr} refer to the rotor inductance, stator inductance, and mutual inductance, respectively. and relate to the leakage inductances of the rotor and stator. and relate to the magnetizing inductance of the rotor and stator. θ_r is the angle formed by the stator and rotor at a given moment.

The flux entering the air gap area is divided into two parts: the mutual inductance inside the stator and the rotor, which is dependent on the rotor position and angle of rotation. As a result, voltage equations for induction motors are affected by the relative angular position of the rotor and stator. Because of its relative angular location, the induction motor's modeling and equations are rather complicated.

a. Reference frame theory

As demonstrated in Equations (11-12), the phase voltage equations obtained in the preceding section incorporate time-dependent differential equations. Reference frames reduce time-varying components, making three-phase machine analysis easier.

Robert Park introduced the reference frame theory in the 1920s, which translates stator variables to a reference frame fixed in the rotor. This variable transformation, also known as Park's transformation, removes time-dependent variables and depicts the voltage values as shown in Equation (18):

$$e_d = \frac{2}{3}\{e_a \cos\theta + e_b \cos(\theta - 120) + e_c \cos(\theta + 120)\}$$
$$e_q = \frac{2}{3}\{e_a \sin\theta + e_b \sin(\theta - 120) + e_c \sin(\theta + 120)\}$$
$$e_0 = \frac{2}{3}\{e_a + e_b + e_c\}$$

(18)

The voltage is represented by e, while the phases are represented by the subscripts a, b, and c. The reference frame's subscripts are designated by d, q, and 0, and the new reference frame is known as the dq0 reference frame. In Equation (19), these three voltage representations in the dq0 reference frame may be reduced into a matrix format.

$$[F_{0dq}] = [P_\theta][F_{ABC}]$$

(19)

$$[P_\theta] = \frac{2}{3} \begin{bmatrix} \frac{1}{2} & \frac{1}{2} & \frac{1}{2} \\ \cos\theta & \cos(\theta - \lambda) & \cos(\theta + \lambda) \\ \sin\theta & \sin(\theta - \lambda) & \sin(\theta + \lambda) \end{bmatrix}$$

P_θ represents the transformation matrix from the *abc* frame to the dq0 reference frame. The zero sequence (e_0) is used to create an invertible square matrix for inverse transformations, such as from the *dq0* frame to the *abc* frame, while also accounting for imbalanced voltages [23].

In contrast to Park's transformation, Stanley proposed a new reference frame focused on the stator rather than the rotor. To avoid time-varying fluxes in the voltage equations, the rotor variables are changed with reference to a fixed frame based on the stator. *Stanley* provided six additional variables to shift the *abc* reference frame to his proposed reference frame: v_α, v_β, v_0, V_α, V_β, and V_0, which are specified in Equation (20):

$$v_0 = \frac{1}{3}(v_1 + v_2 + v_3)$$

$$v_\alpha = \frac{2}{3}\left[v_1 \cos\theta + v_2 \cos\left(\theta + \frac{2\pi}{3}\right) + v_3 \cos\left(\theta - \frac{2\pi}{3}\right)\right]$$

$$v_\beta = \frac{2}{3}\left[v_1 \sin\theta + v_2 \sin\left(\theta + \frac{2\pi}{3}\right) + v_3 \sin\left(\theta - \frac{2\pi}{3}\right)\right]$$

$$V_0 = \frac{1}{3}(v_a + v_b + v_c)$$

$$V_\alpha = \frac{2}{3}\left[v_a - \frac{1}{2}(v_b - v_c)\right]$$

$$V_\beta = \frac{\sqrt{3}}{2}(v_b - v_c)$$

(20)

Kron [25] proposed a synchronous rotating reference frame for rebuilding stator and rotor variables to be coordinated with the spinning magnetic field. Krause [26] introduced the arbitrary reference frame as a more complete reference frame for combining diverse transformations into a single universal transformation [26], [22]. By translating the stator and rotor variables to a stationary or rotating reference frame, the arbitrary reference frame eliminates all time-varying variables.

b. Arbitrary reference frame

Given the transformation matrix K_s, Equation (21) expresses the transformation of variables from the conventional *abc* frame to the arbitrary reference frame *dq0*.

$$f_{qd0s} = Ksf_{abcs} \qquad (21)$$

where *fqd0s* denotes the altered variables in the arbitrary reference frame and denotes the variables in the *abc* reference frame Equation (22) defines the transformation matrix Ks:

$$K_s = \frac{2}{3}\begin{bmatrix} \cos\theta & \cos\left(\theta - \frac{2\pi}{3}\right) & \cos\left(\theta + \frac{2\pi}{3}\right) \\ \sin\theta & \sin\left(\theta - \frac{2\pi}{3}\right) & \sin\left(\theta + \frac{2\pi}{3}\right) \\ \frac{1}{2} & \frac{1}{2} & \frac{1}{2} \end{bmatrix} \qquad (22)$$

The Inverse is:

$$K_s^{-1} = \begin{bmatrix} \cos\theta & \sin\theta & 1 \\ \cos\left(\theta - \frac{2\pi}{3}\right) & \sin\left(\theta - \frac{2\pi}{3}\right) & 1 \\ \cos\left(\theta + \frac{2\pi}{3}\right) & \sin\left(\theta + \frac{2\pi}{3}\right) & 1 \end{bmatrix} \tag{23}$$

Where, $\theta = \int \omega dt$; it is the angular velocity

This transformation may be used on any variable, including voltage, current, flux connections, and electric charge. The angular velocity defines an arbitrary rotation of the reference frame, which transforms all other variables. There are three typical transformations based on the rotation of the reference frame. Clark's transformation occurs when the reference frame is stationary, i.e. the angular velocity is zero. Park's transformation is a transformation with regard to a revolving rotor in which the angular velocity is specified by that of the rotor. The transformation is known to involve the synchronous reference frame if the angular velocity of the reference frame is set to the synchronous speed .

c. Types of reference frames

Stationary reference frame: A stationary reference frame is one in which the axes, d, and q are fixed at a fixed position. Clark's transformation in the stationary reference frame employs the notations: f_α, f_β and f_0 for the changed variables.

Three phase variables (a, b, c) are projected onto orthogonal axes d_s and q_s fixed on the stator in the stationary reference frame, as illustrated in Figure 3. For the sake of simplicity, one of the stationary variables is assumed to be collinear with the x-axis.
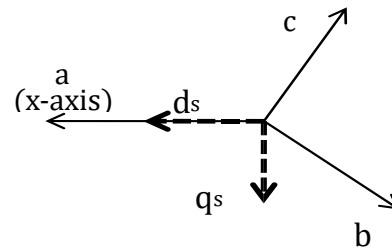

Figure 3 : Vector diagram for the stationary reference frame

Because the angular velocity is zero, the transformation statement becomes:

$$\begin{bmatrix} f_\alpha \\ f_\beta \\ f_0 \end{bmatrix} = \frac{2}{3} \begin{bmatrix} 1 & \frac{-1}{2} & \frac{-1}{2} \\ 0 & \frac{\sqrt{3}}{3} & \frac{-\sqrt{3}}{3} \\ \frac{1}{2} & \frac{1}{2} & \frac{1}{2} \end{bmatrix} \begin{bmatrix} f_a \\ f_b \\ f_c \end{bmatrix} \tag{24}$$

The variables in the stationary reference frame are denoted by the subscripts α, β and 0. The variable that is balanced in the *abc* reference frame is the zero sequence component, $f_0=0$. As seen in Figure 3, this turns three input variables into two orthogonal variable representations.

Rotor Reference Frame: The reference frame is considered to be fixed in the rotor if it rotates at the same speed as the rotor $\omega = \omega_r$. This reference frame, like a three-phase rotor, will have an a-phase axis. Because the reference frame is based on the rotor, the *d-axis* of the frame will be collinear with the a-phase axis of the rotor, as seen in Figure 4.
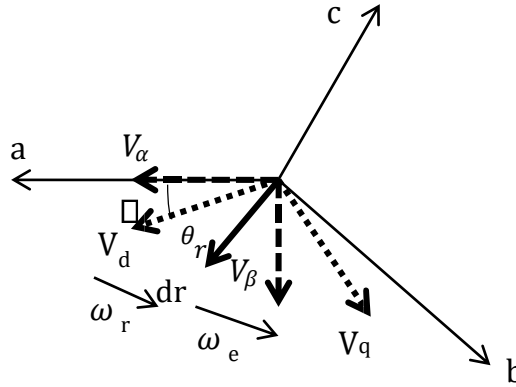

Figure 4 : Representation of the rotor reference frame

Variables in the stationary reference frame q_s-d_s are transformed to the rotor reference frame q_r-d_r using a rotation transformation matrix given by the angle between two frames:

$$\begin{bmatrix} v_q^r \\ v_d^r \end{bmatrix} = \begin{bmatrix} \cos(\theta_e + \theta_r) & -\sin(\theta_e + \theta_r) \\ \sin(\theta_e + \theta_r) & \cos(\theta_e + \theta_r) \end{bmatrix} \begin{bmatrix} v_q^s \\ v_d^s \end{bmatrix} \tag{25}$$

Synchronous rotating reference frame: In Figure 5, the stationary variables are represented in relation to a reference frame that rotates at a synchronous speed ($\omega=\omega_s$).
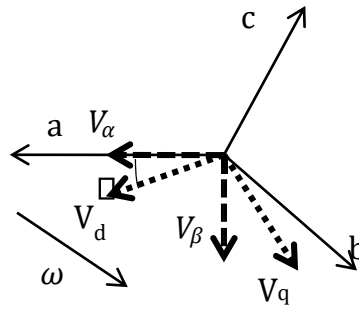

Figure 5 : Representation of the Synchronous rotating reference frame

Equation 26 gives the transformation from the stationary reference frame q_s, d_s to the synchronously rotating reference frame (q^k, d^k) subject to a rotation angle.

$$\begin{bmatrix} v_q^k \\ v_d^k \end{bmatrix} = \begin{bmatrix} \cos\theta & -\sin\theta \\ \sin\theta & \cos\theta \end{bmatrix} \begin{bmatrix} v_q^s \\ v_d^s \end{bmatrix} \qquad (26)$$

Arbitrary reference frame equations: Using the voltage and linkage flow equations, the equivalent circuit model of the induction motor, as shown before, is utilized to generate the appropriate equations in the arbitrary reference frame.
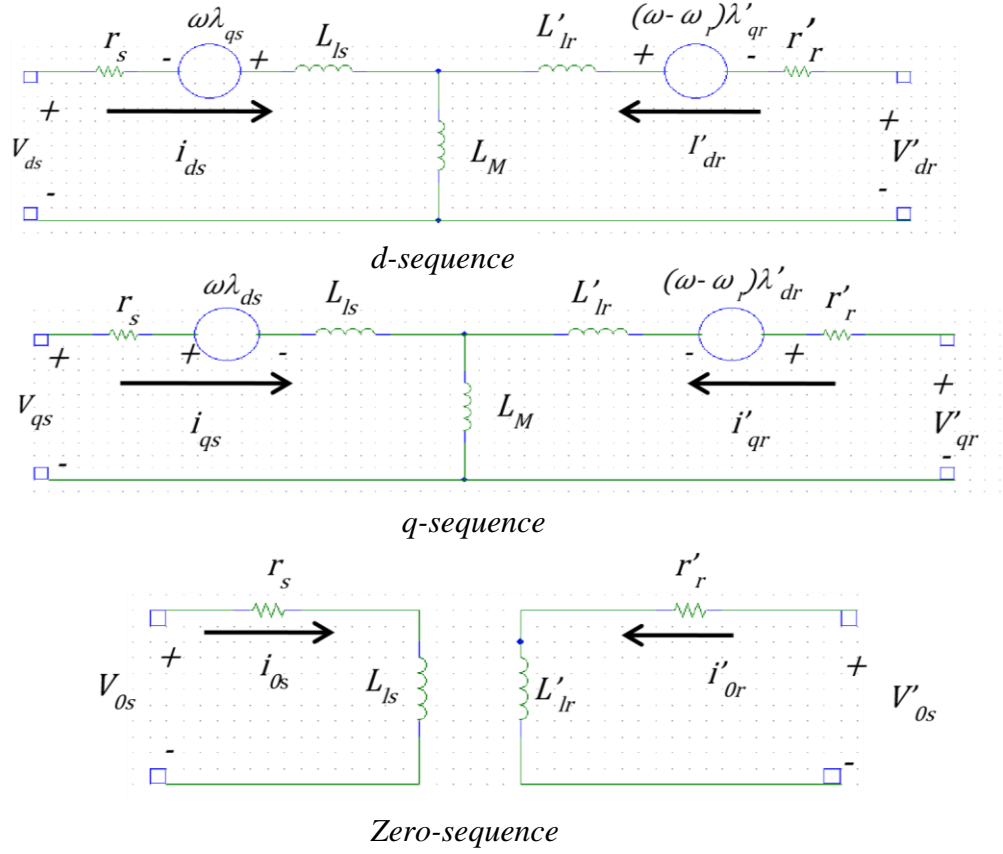
d-sequence

q-sequence

Zero-sequence

Figure 6 : Equivalent circuit of an IM in the arbitrary reference frame dq0

The differential equations for the stator and rotor flux linkages are solved using Figure 6 by referring to a reference frame at an arbitrary angular velocity, as shown in Equations (27-28), where r is the electrical angular velocity and is the reference frame angular velocity:

Currents may alternatively be described as a function of flux linkage using the flux linkage equations by replacing Equation (28) with Equation (27):

$$
\left.
\begin{aligned}
v_{qs} &= r_s i_{qs} + \frac{d\lambda_{qs}}{dt} + \omega\lambda_{ds} \\[4pt]
v_{ds} &= r_s i_{ds} + \frac{d\lambda_{ds}}{dt} - \omega\lambda_{qs} \\[4pt]
v'_{qr} &= r'_r i'_{qr} + \frac{d\lambda'_{qr}}{dt} + (\omega - \omega_r)\lambda'_{dr} \\[4pt]
v'_{dr} &= r'_r i'_{dr} + \frac{d\lambda'_{dr}}{dt} + (\omega - \omega_r)\lambda'_{qr}
\end{aligned}
\right\} \qquad (27)
$$

$$\lambda_{ds} = L_s i_{ds} + L_m i'_{dr}$$

$$\lambda_{qs} = L_s i_{qs} + L_m i'_{qr}$$

$$\lambda'_{qr} = L'_r i'_{qr} + L_m i_{qs}$$

$$\lambda'_{dr} = L'_r i'_{dr} + L_m i_{ds}$$

$$(28)$$

$$i_{qs} = \frac{L_r \lambda_{qs} - L_m \lambda'_{qr}}{L_r L_s - L_m^2}$$

$$i_{ds} = \frac{L_r \lambda_{ds} - L_m \lambda'_{qr}}{L_r L_s - L_m^2}$$

$$i'_{qr} = \frac{L_s \lambda'_{qr} - L_m \lambda_{qs}}{L_r L_s - L_m^2}$$

$$i'_{dr} = \frac{L_r \lambda'_{qr} - L_m \lambda_{dr}}{L_r L_s - L_m^2}$$

$$(29)$$

Table 2 : Angular position and difference summary of the reference frame

Reference frame	θ_r	β
Rotor	θ	0
Stationary	0	$-\theta_r$
Synchronous	θ_e	θ_e-θ_r

There are several methods to express electromagnetic torque and rotor speed. The equations provided in Equations (30-31) [27] are the most usually used:

$$T_e = \frac{3}{2}\frac{P}{2}\left(\lambda_{ds}i_{qs} - \lambda_{qs}i_{ds}\right) \qquad (30)$$

$$\omega_r = \int \frac{P}{2J}(T_e - T_L) \qquad (31)$$

According to the preceding equations, is equal to the number of poles and represents the moment of inertia value.

The moment of inertia J and the flywheel effect GD^2 are used to explain the moment of inertia. The fly wheel effect is frequent in industrial applications with unit *Kgf.m* and is four times bigger than value J. The flywheel effect of the motor is acquired from the Toshiba catalog for the 3P-IM, which is 0.01, where the frame number is D71M. The link between J and GD^2 is provided by

$$J = \frac{GD^2}{4} = 0.0025 kg.m^2 \tag{32}$$

IV.   Torque speed characteristics

Torque-speed characteristics are critical elements in the operation and performance of an induction motor. Three zones between stationary and synchronous speed can be used to explain the torque-speed characteristics of a 3P-IM. This range is represented fractionally by the slip (s), which is the slip speed to synchronous speed ratio. Within this complete speed range, the effective torque may be divided into three slip regions: low slip, moderate slip, and high slip. As shown in Figure 7, each zone corresponds to a distinct operating state of the motor in terms of torque.
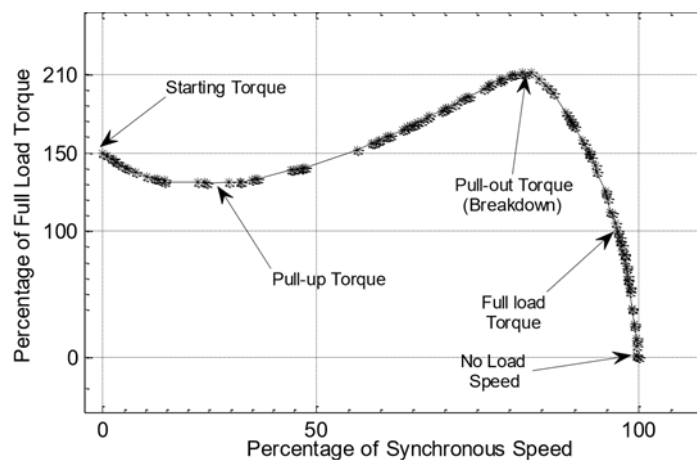

Figure 7 : Torque-Speed characteristics of a 3IM

The pull-out torque of an induction motor can be two to three times the machine's nominal full load torque. In contrast, the initial torque may be merely 150 percent of the entire load torque [20].

a. Low-slip region

In the low slip area, the slip of the motor increases linearly proportional to the torque. However, when the slip increases, the motor speed decreases. Due to a negligible rotor reactance, the power factor remains almost constant in the low slip zone, where the current grows in direct proportion to the slip. This area contains the motor's regular steady-state functioning range. Under normal conditions, an induction motor's speed decreases linearly with load.

b. Moderate-slip region

As the mechanical speed of the motor lowers with increased load, it moves from the low slip zone to the moderate slip zone. When compared to the low-slip zone, the frequency is greater in the moderate-slip region. The amount of the rotor's reactance and resistance, on the other hand, stays constant. The rotor current does not grow as quickly as it does in the low slip area. Once the rotor current increases, the pull-out torque situation (maximum torque) occurs in this area to offset the rotor power factor fall.

c. High-slip region

With a further rise in load, the motor enters the high slip area, where it experiences a drop in speed with a commensurate increase in load. This occurs when the motor's power factor decreases more than the rotor current increases. When the rotor drive is forced to spin faster than the synchronous speed (Ns > Nm), the slip is negative and the torque direction is reversed, changing the motor into a generator and converting mechanical power to electrical power.

V. Symmetrical Component

A balanced power system combines a three-phase supply voltage of equal magnitude in each phase, with each phase separated by a phase angle of 120° from the others. An imbalanced condition develops when there is a disparity in the amplitude and phase of the supply voltage. The symmetrical component technique well understands, analyzes, and explains the influence of an imbalance on a 3P-IM operation. This approach provides for the quick and accurate estimation of currents and voltages that contribute to imbalanced situations.

An imbalanced 3P-IM may be examined using three voltage sequences: the negative sequence, the positive sequence, and the zero sequence. In the event of unbalanced voltages, the 3P-IM is thought to be comparable to two identical induction motors installed on the same shaft, with the positive and negative sequences acting as two independent motors in principle. The positive sequence voltage produces torque in the direction of primary rotation as if the motor were working under balanced circumstances. In other words, positive sequence components are merely voltage, current, and impedances from a balanced system. The negative sequence, on the other hand, generates torque in the opposite direction of the primary rotation. The negative sequence voltage becomes dominant and substantial as the degree of imbalance increases because it provides an air gap flux that counteracts the primary rotation of the motor. Because of the low negative sequence impedance, the resulting current is considerable. This research only includes 3P-IMs with wye connections and no neutral path.

Regarding the effects on operational characteristics, the negative sequence currents and voltages are essentially the results of unbalanced voltage conditions, whereas under balanced conditions only the positive sequence components are present. The negative sequence components counteract the real throughput of the motor and contribute to power loss and generate excessive heat. The rotor losses are increased due to the breakdown of voltage and currents into positive and negative sequences. Unbalanced conditions also contribute to positive sequence voltage drops which result in an increase in the positive sequence current within the stator and rotor, generating excessive heat.

The temperature rises as a result of the heat created by the negative sequence components. Figure 8 depicts how the temperature rises exponentially as the proportion of voltage imbalance increases. As a result, precautionary measures are required to avoid the possibility of the motor being destroyed due to the growth in temperature.
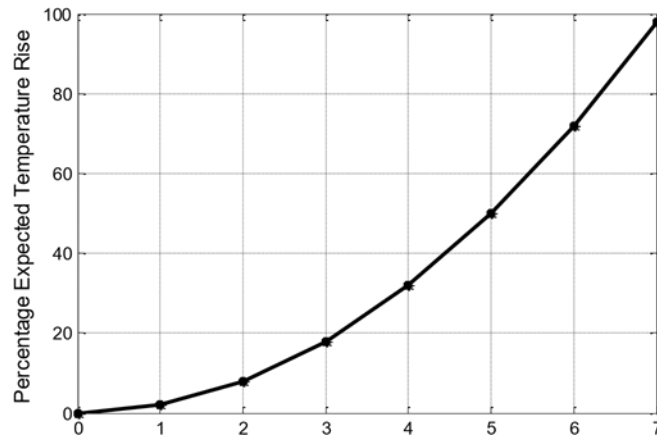
Figure 8 : Percentage temperature rise versus percentage voltage imbalance in an induction motor

Voltage imbalance influences mechanical output torque by altering the blocked-rotor pull-up and breakdown torques, as represented in the torque-speed characteristic curve shown in Fig. 7. Even if the motor survives extreme situations of imbalance, the output torque provides little practical advantage. When the motor runs in imbalanced conditions, the full-load speed decreases somewhat.

VI. The Equivalent Circuit Diagram

In imbalanced conditions, the induction motor functions like two independent motors operating in parallel. Two equivalent circuits based on positive and negative sequence components may be used to describe these equivalent induction motors. The positive sequence components are derived from a balanced induction motor representation. As a result, the equivalent circuit for positive sequence components is the same as before and is depicted in Figure 9.
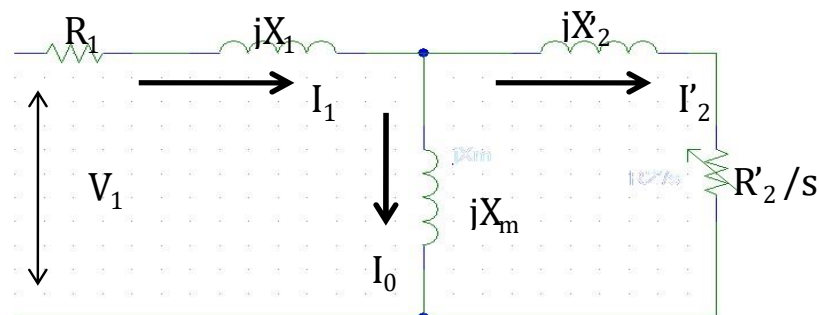

Figure 9 : Unbalanced voltage equivalent circuit for the positive sequence

The negative sequence equivalent circuit is nearly identical to the positive sequence equivalent circuit, with the exception of a variable slip on the rotor side, as illustrated in Fig. 10. The shift in slip is generated by the negative sequence's counteracting torque working against the positive sequence's torque. The negative sequence slip is determined using Equation 3:

$$S_+ = \frac{Ns - Nr}{Ns}$$

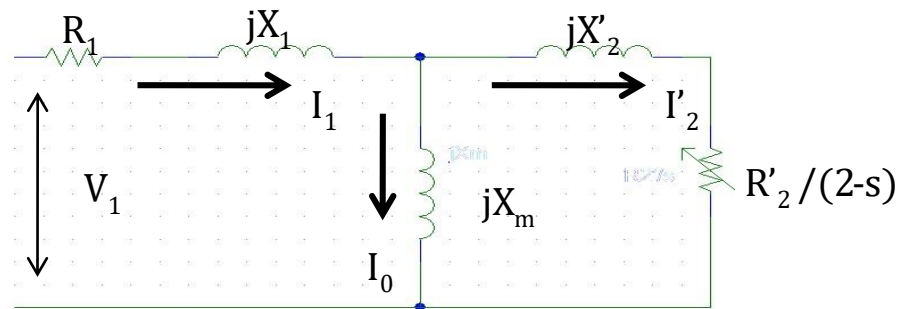$$S_- = \frac{-Ns - Nr}{-Ns} = \frac{Ns + Nr}{Ns} = \frac{2Ns - (Ns - Nr)}{Ns} = 2 - S_+$$

Figure 10 : Unbalanced voltage equivalent circuit for the negative sequence

> **Degrees of Unbalanced Standards**

The degree of imbalance is referred to in many Australian Standards produced by 'Standards Australia' and the National Equipment Manufacturer's Association (NEMA). These standards are critical in developing the appropriate safeguards for electrical machinery and preventing dangerous imbalanced situations.

These standards were used in this study to determine the essential measurements for imbalanced voltage conditions.

> **Percentage Voltage Imbalance (PVI)**

When the voltage imbalance is 5% higher than the average, the study of negative sequence components becomes critical. Similar to NEMA's voltage unbalanced rate (LVUR). The LVUR – NEMA standard was chosen because it takes the phase angle into account in the average line voltage imbalance, whereas the Institute of Electrical and Electronics Engineers (IEEE) does not.

$$LVUR\text{–}NEMA = \frac{Maximum\ voltage\ deviation\ from\ average\ line\ voltage\ magnitude}{Average\ line\ voltage\ magnitude} * 100\%$$

(33)

The calculation above provides an approximation of the proportion of the negative sequence voltage component. The true negative sequence voltage component can be up to 18% higher than the approximation amount. Symmetrical components are examined in order to offer a more accurate assessment of negative sequence voltage components that may result in imbalanced circumstances.

> **Voltage Unbalance Factor (VUF) and Derating Curve**

According to Standards Australia, if an AC motor is connected to a three-phase voltage supply with a negative sequence component that outstrips 1% of the positive sequence component voltages for an extended period of time, the allowable motor power is reduced so that it is less than the rated power to protect the motor from potential damage. Figure 11 depicts a derating curve for motors of design class N, which reproduces the derating factor versus the voltage imbalance factor from NEMA. IEC Design N motors are similarly comparable to NEMA Design B motors, which are the most popular industrial motors.

$$\text{VUF} = \frac{Negative\ sequence\ voltage\ component\ (unbalanced)}{Positive\ sequence\ voltage\ component} * 100\% = \frac{Un}{Up} * 100 \qquad (34)$$

Where *Un* and *Up* are the RMS values of the supply voltage's negative and positive sequence components, respectively. A VUF of more than 5% is not recommended for motor operation, which equates to around 75% of the derating factor indicated in Figure 11.
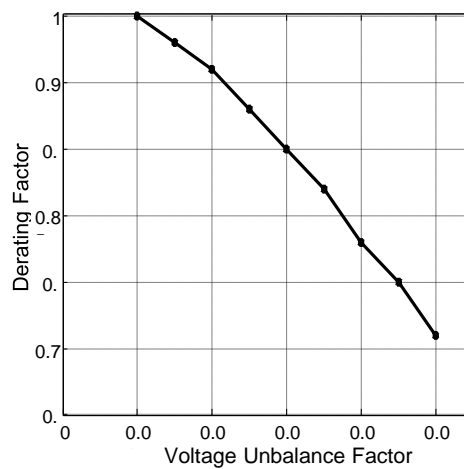

Figure 11 : Derating curve of an IM design class N

Chapter 3 : Methodology

I.   Motor Parameters

i.   DC Test

The DC test seeks to determine stator resistance R_1, which is then used to calculate rotor resistance R_2. The rotor resistance is critical because it results in distinct motor characteristics from the torque-speed characteristic curve. The induction motor is powered by a direct current voltage. Because there is no induction of flux into the rotor due to zero frequency, there is no induced voltage, current, or reactance. As illustrated in Figure 12, the DC power source is connected to two of the three phases of the 3P-IM. In this configuration, the voltage is adjusted to set the line current to be close to or equal to the rated current of the motor in order to establish normal operating temperature in the motor.
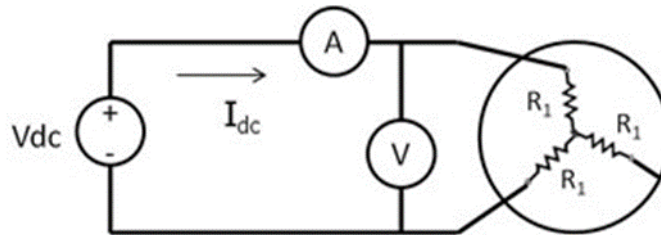

Figure 12: Circuit Diagram for the DC Test

Because the current passes via two windings of the stator, the total resistance in the current path is 2R1. R1 is simply calculated from the supply voltage and resulting current.

Using the connection schematic in Figure12, execute the DC test on an induction motor as per the laboratory recommendations.

$$R1= \frac{Vdc}{2Idc} \qquad\qquad\qquad (35)$$

ii.   Blocked-rotor Test

The stator resistance measured in the DC test is utilized to calculate the stator and rotor reactance variables X1 and X2 in the blocked-rotor test. The rotor is blocked in this test to provide full load on the shaft. In this situation, a plate attachment was used to secure the rotor. Following the locking of the rotor, a three-phase voltage was applied to the motor, and the resulting power, voltage, and current values were determined for each phase, as shown in Figure13. The values from the three phases were averaged.
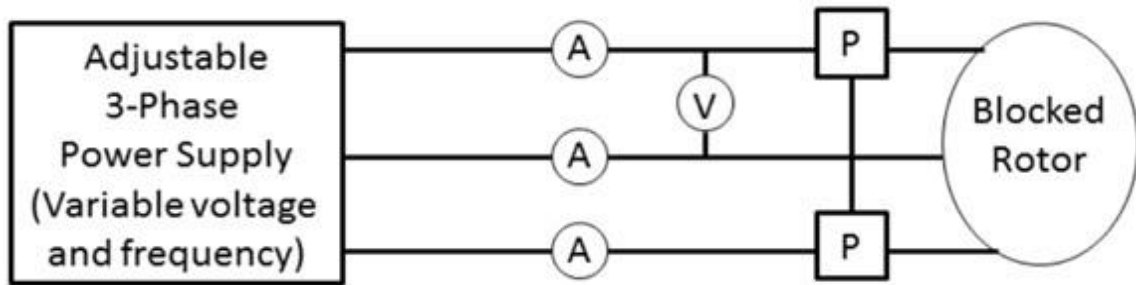

Figure 13 : Circuit Diagram for the Blocked Rotor Test

The blocked-rotor test necessitates the application of an alternating current power source to the stator, after which the current flow was adjusted to roughly full-load value. Once the current had achieved its rated value, the voltmeter, ammeter, and power meter measurements were taken. The stator and rotor reactance values were calculated using the experimental measurements. Although the stator and rotor reactance values are interrelated, empirical results allow them to be separated.

The mechanical speed is zero when the rotor is blocked, indicating that the slip is at unity. As a result, the rotor current exceeds the exciting current, which may then be ignored. Figure 14 depicts the corresponding per-phase circuit diagram under blocked rotor test circumstances.
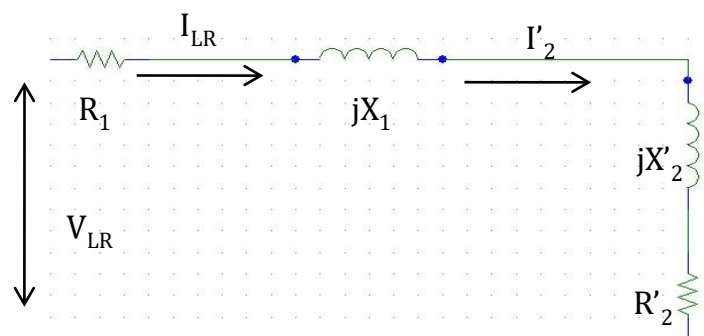

Figure 14 : Equivalent circuit under block rotor test (per phase)

Using Equation (36), the rotor winding resistance may then be estimated from the power meter and ammeter measurements.

$$P_R = 3 * I^2_{LR} * (R1 + R2) \tag{36}$$

$$Z_R = \frac{V_{LR}}{I_{LR}} = \sqrt{(R_1 + R_2)^2 + (X_1 + X_2)^2} \tag{37}$$

Equation (37) gives the result $X = X_1 + X_2$. Individual values for X_1 and X_2 for different kinds of motors can be derived using the NEMA-specified empirical formula. The IEC Torque-Speed design parameters are nearly comparable to those in the NEMA standards. According to the NEMA standard for class B motors, $X_1 = 0.4\ X$ and $X_2 = 0.6\ X$, where $X = X_1 + X_2$.

The rotor and stator reactance equations can alternatively be rearranged as follows:

$$X_1 = 0.40 * \frac{Q_{RL}}{I^2_{RL}} \tag{38}$$

$$X_2 = 0.60 * \frac{Q_{RL}}{I^2_{RL}} \tag{39}$$

Given the value of X1, the magnetizing reactance may be estimated from the blocked-rotor test.

iii. No-Load Test

The primary objective of doing the no-load test is to establish the motor's magnetization reactance, XM. Unlike the blocked-rotor test, the rotor is assumed to spin freely without any weight or attachment. The test also evaluates the losses caused by the motor's rotation. Only core losses are included in this analysis since they account for the majority of the losses. Because the rotor current (I_2) is so low under no-load situations, copper losses are likewise deemed insignificant.

The motor is activated differently during the no-load test than during the blocked-rotor test. The primary goal here is to set the voltage and frequency to their rated levels rather than the current. As illustrated in Figure 15, the voltage, current, power, and frequency for each phase are monitored. The measured values are averaged throughout the three stages, as in the blocked-rotor test.
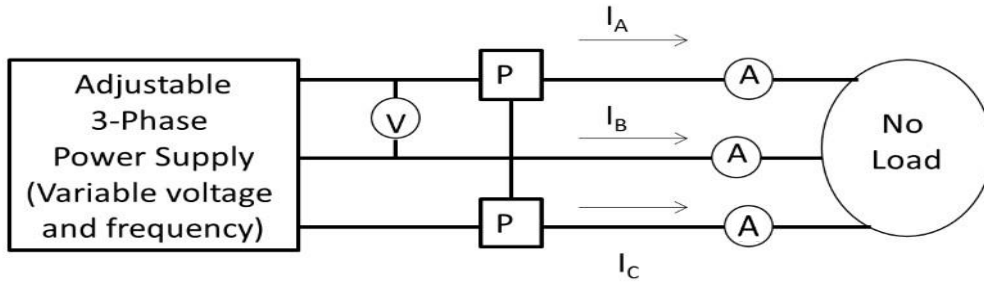
Figure 15 : Circuit diagram for the No-Load test

The no-load test is used to measure the motor's rotational losses and offers additional data to calculate the magnetization reactance. The following procedures are based on the circuit design illustrated in Figure 16:
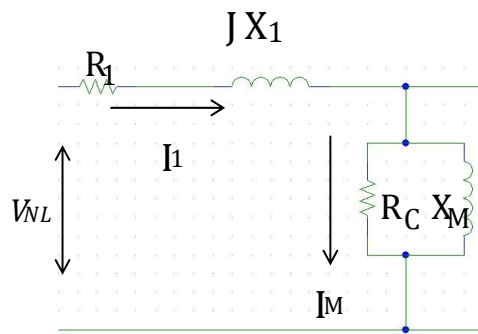

Figure 16 : Circuit diagram under no-load test (per phase)

✓ The circuit is built as illustrated in Figure 15, with the ammeters following the power meters. Turn on the variable power supply and measure the voltage (V_{NL}), input power (P_{NL}), and stator current (I_{NL}). The variable supply is then disconnected.

✓ The magnetizing reactance (X_M) is calculated by subtracting the stator reactance (X_1) from the blocked rotor test from the no-load reactance (X_{NL}). The power triangle may be used to calculate reactive power (Q_{NL}) from the no-load test, as shown in Equation (40):

$$Q_{NL} = \sqrt{(V_{NL} * I_{NL})^2 - P_{NL}^2} \qquad (40)$$

Finally, we will get:

$$X_{NL} = \frac{Q_{NL}}{I^2_{NL}} \qquad (41)$$

$$X_M = X_{NL} - X_1 \qquad (42)$$

After obtaining all of the essential data for the motor model from the three tests, this model and the model parameters may be used to simulate the performance of the 3P-IM under various loads or supply voltage situations.

Table 3 : Results for all the tests

	DC test	Blocked rotor test	No-load test
Average Voltage (per phase)	26.4 V	55.2 V	241 V
Average Current	1.09 A	1.09 A	0.7 A
Average Real power	28.34 W	34.8 W	17.2 W
Reactive Power	16 VA	63.4 VA	170.5 VA
Frequency	0 Hz	49.99 Hz	50 Hz

II.   Simulation of the three-phase Induction Motor

a. Simulink Overview

Simulink was used to simulate a 3P-IM using a synchronous motor model. Simulink is a graphical extension built into MATLAB that provides appropriate libraries and analytical tools, including several models for simulating three-phase machines, electric motors, and other comparable electrical systems. It includes an Asynchronous Machine block that may be customized to represent the dynamics of a three-phase induction motor. It also enables the modeling of a three-phase transition to an arbitrary reference frame to represent transient behavior. Simulink has a variety of engineering toolboxes and features that have been used by a large number of researchers in electrical machines and power systems. Due to the formation of DC parameters in the rotor and stator d, q variables, past simulation experiences have revealed that the synchronous reference frame is the best for modeling induction motors. The transient and steady-state properties of a 3P-IM, as well as the torque-speed characteristics, are compared in various reference frames. The Simulink simulation model contains four inputs: mechanical torque and three input line-to-line voltages. Electromagnetic torque, rotor speed, rotor currents, and stator currents are the outputs. In Simulink, the induction model uses the arbitrary reference frame theory to analyze the performance of the 3PIM during an electrical failure. Faults were induced in this simulated environment, and fluctuations in motor output related to a defective state were detected.

Depending on the mechanical torque value, an asynchronous machine can operate in either motor or generator mode. This number is a positive constant in a motor model. The full energy conversion system is represented by both electrical and mechanical models. Two lists of observations were made using two functionally separate blocks: electrical and mechanical. In these blocks, all equations were implemented. The electrical model is divided into numerous subsystems. It first transforms voltages from the *a-b-c* system to a *d-q* system, and then one of the components employs sine and cosine transformations from the *d-q* system to the *a-b-c* system. The other section transforms currents, while the third section converts fluxes to the *d-q* system. One of the subsystems computes all direct and quadrature axis currents, as well as mutual fluxes.

b. Model of the Induction Motor in Simulink

Simulink, which is based on MATLAB, has a dynamic model for an induction motor that may be customized. This model is made up of multiple sub-models. As previously mentioned, the electrical sub-model converts the three-phase electrical variables to the two-axis *dq* reference frame. The torque sub-model calculates the produced electromagnetic torque, whereas the mechanical sub-model calculates the rotor speed. A stator current output sub-model is also developed to calculate line voltage decreases.

i. Electrical Sub-model

The Electrical sub-model converts three-phase voltages or currents to a two-axis *d-q* representation, as shown in Equation (43):

$$\begin{bmatrix} V_{ds} \\ V_{qs} \end{bmatrix} = \begin{pmatrix} 1 & \frac{-1}{2} & \frac{-1}{2} \\ 0 & \frac{\sqrt{3}}{2} & \frac{-\sqrt{3}}{2} \end{pmatrix} * \begin{bmatrix} V_{as} \\ V_{bs} \\ V_{bs} \end{bmatrix} \tag{43}$$

Where *s* denotes the stator, *abc* indicates the three phases, and d and q denote the *d-q* reference frame. Figure 17 depicts the electrical sub-model blocks.
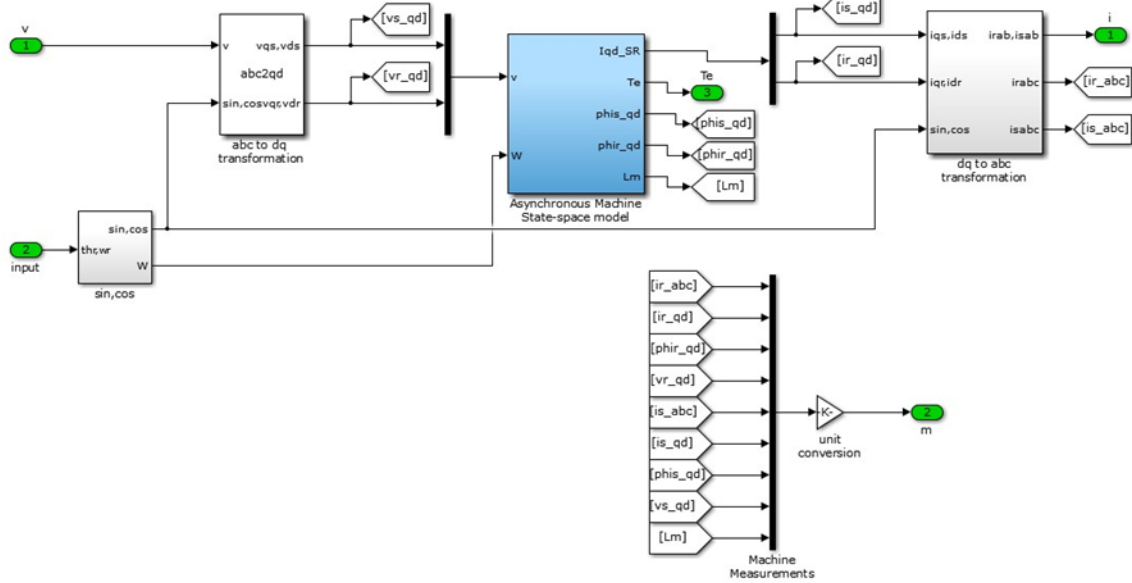
Figure 17 : Electrical Sub-model using Simulink

Here, inputs are *dq* components of stator and rotor: $u[1]=i_{ds}$; $u[2]=i_{qs}$; $u[3]=i_{dr}$; $u[4]=i_{qr}$. Angular frequency $u[5]=\omega_0$.

The transformation matrix for the synchronous reference frame may be constructed in Simulink using four function blocks, as illustrated in Figure 18. The inputs to the electrical sub-model are three-phase voltages in the *abc* reference frame that are translated to current vectors [i_{ds}, i_{qs}, idr, i_{qr}] that reflect the stator and rotor currents in the *d-q* reference frame.
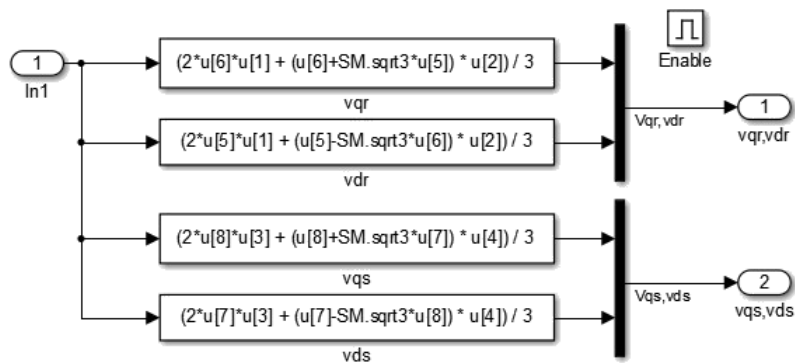
Figure 18 : System implemented with Simulink

ii. Torque sub-model

Once the electrical variables in the *dq* reference frame have been determined using the electrical sub-model, the transformed stator (i_{ds}, i_{qs}) and rotor (i_{dr}, i_{qr}) currents are utilized to compute the induced electromagnetic torque (T_e) in the torque sub-model by rearranging Equation (30) [36]:

$$T_e = \frac{PL_m}{3}\left[i_{dr}i_{qs} - i_{qr}i_{ds}\right] \tag{45}$$

where P represents the rated input power and L_m represents the magnetization inductance. Mechanical sub-model of an induction motor: The rotor angular speed (ω_0) may be calculated from the induced electromagnetic torque (T_e) by ignoring viscous friction, as shown in Equation (46) [36]:

$$\omega_0 = \int_{T=0}^{t} \frac{T_e - T_L}{J} dT \tag{46}$$

Where J is the rotor's moment of inertia and T_L is the load torque.

iii. Stator Current Sub-model

$$|i_s| = \frac{2}{3}\sqrt{i_{qs}^2 + i_{ds}^2} \tag{47}$$

The electromagnetic torque is calculated by transforming the stator fluxes and current components into *dq* reference frame values. Equations (45-47) show the solutions to the essential equations. The Simulink blocks for the mathematical procedure underpinning the T_e computation are shown in Figure 19.
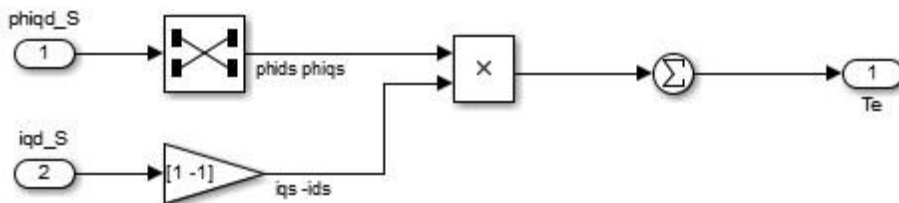

Figure 19 : Electromagnetic torque using Simulink

$Te = phids * iqs - phiqs * iqs$, where dq components of the flux produced in the stator, such as and, are estimated from stator inductance and stator-rotor mutual inductance, as indicated in Equation (48) [36]:

$$phiqs = L_s \times i_{qs} + L_m \times i_{qr}$$

$$phids = L_s \times i_{ds} + L_m \times i_{dr}$$

$$(48)$$

iv. Power Supply Sub-model

This sub-model comprises a three-phase voltage generator and calculates terminal voltage depending on line voltage drop. The terminal voltages after cable drops have a magnitude of $|V|$ following a drop in the produced voltage E from cable resistance R_c due to stator current $|is|$.
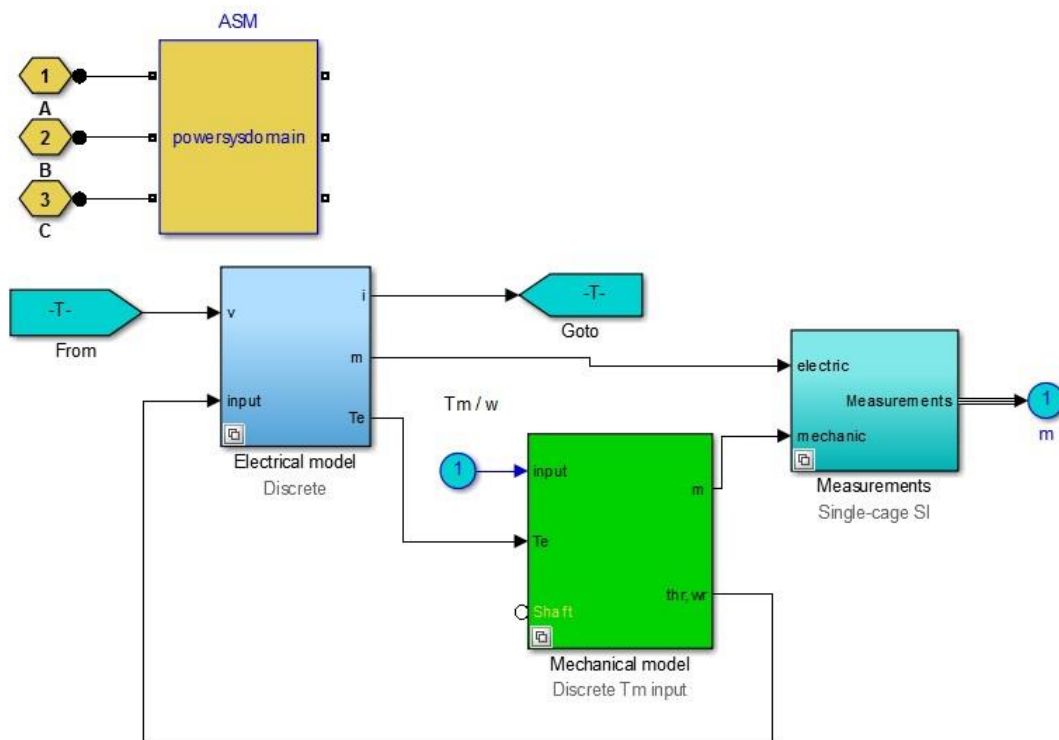

Figure 20 : Overall setup for the Sub-system of the Asynchronous model

Chapter 4 : Experimental Results

I.   Parameters estimation

The electrical parameters for the 3P-IM were computed using MATLAB from the DC test, the blocked-rotor test, and the no-load test:

Table 4 : Parameters obtained after compilation with Matlab

Stator resistance	Rotor resistor	Stator reactance	Rotor reactance	Stator inductance	Rotor inductance	Magnetizing reactance	Magnetizing inductance
R_1=12.05Ω	R_2=12.9Ω	X_1=16.7Ω	X_2=25.15Ω	L_1=0.05H	L_2=0.08H	X_M=325.7Ω	L_M=1.03H

II.   Simulation results

For a fixed frictional torque and given the output shaft power (P_o) and angular frequency of rotation (ω_m), the torque (T_L) under load is determined by rearranging Equation (8):

$$T_L = \frac{P_0}{\omega_m}$$

Ns at zero slip, s = 0, the angular speed (ω_s) is given by:

$$\omega_s = \frac{2\pi N_s}{60} = \frac{2\pi * 1500}{60} = 157.10 \; rad/s$$

N_r=1410 rpm; N_s=1500 rpm;

By using Equation (3), the slip (S) is:

$$S = \frac{N_s - N_r}{N_s} = \frac{1500 - 1410}{1500} = 0.06$$

As a result, the rotor's angular speed at rated 6 percent slip is 157.1 (1-s) = 157.1 0.94 = 147.67 rad/sec. The motor has a 370W output power. As a result, Po = 370 W, and the output torque is:

$T_L = \frac{P_0}{\omega_m} = \frac{370}{147.67} = 2.505 Nm$

The following unbalanced voltage circumstances were implemented in Simulink:

- ✓ Magnitude Decrease (Amplitude Vc = 10% Decrease)
- ✓ Magnitude Increase (Amplitude Vc = 10% Increase)
- ✓ Phase Decrease (Phase Vc = 3% Decrease).
- ✓ Phase Increase (Phase Vc = 5% Increase)

✓ Magnitude and Phase Decrease (Amplitude Vc = 10%, Phase Vc = 3% Decrease)

✓ Magnitude and phase Increase (Amplitude Vc = 10%, Phase Vc = 3% Increase)

✓ Phase loss (Vc phase voltage) in a three-phase supply.

These modifications were chosen to give a wide variety of possible unbalanced states and to produce derating factors for motors operating under these varied unbalanced conditions.

Table 5 : Different conditions of the three-phase supply

Parameters	Phase$_i$V$_a$	Phase$_i$V$_b$	Phase$_i$V$_c$
Balanced Condition	**240∠0°**	**240∠-120°**	**240∠-240°**
Magnitude Decrease	240∠0°	240∠-120°	216∠-240°
Magnitude Increase	240∠0°	240∠-120°	264∠-240°
Phase Decrease	240∠0°	240∠-120°	240∠-232.8°
Phase Increase	240∠0°	240∠-120°	240∠-252°
Magnitude and Phase Decrease	240∠0°	240∠-120°	216∠-232.8°
Magnitude and Phase Increase	240∠0°	240∠-120°	264∠-247.2°
Phase loss	240∠0°	240∠-120°	Not connected

Figure 21 shows the Simulink implementation of the experimental setup. The asynchronous machine module is displayed in the center, and it is also configured with the essential parameter values for rated specs, resistances, impedances, and moment of inertia. The three-phase supply connections are shown on the left side of Figure 21 with varied values to represent balanced and unbalanced voltage circumstances. On the rightmost side, many scopes were attached, and the output terminals exhibited various throughputs such as peak magnitude of each voltage, rotor speed, stator/rotor current, and electromagnetic torque.
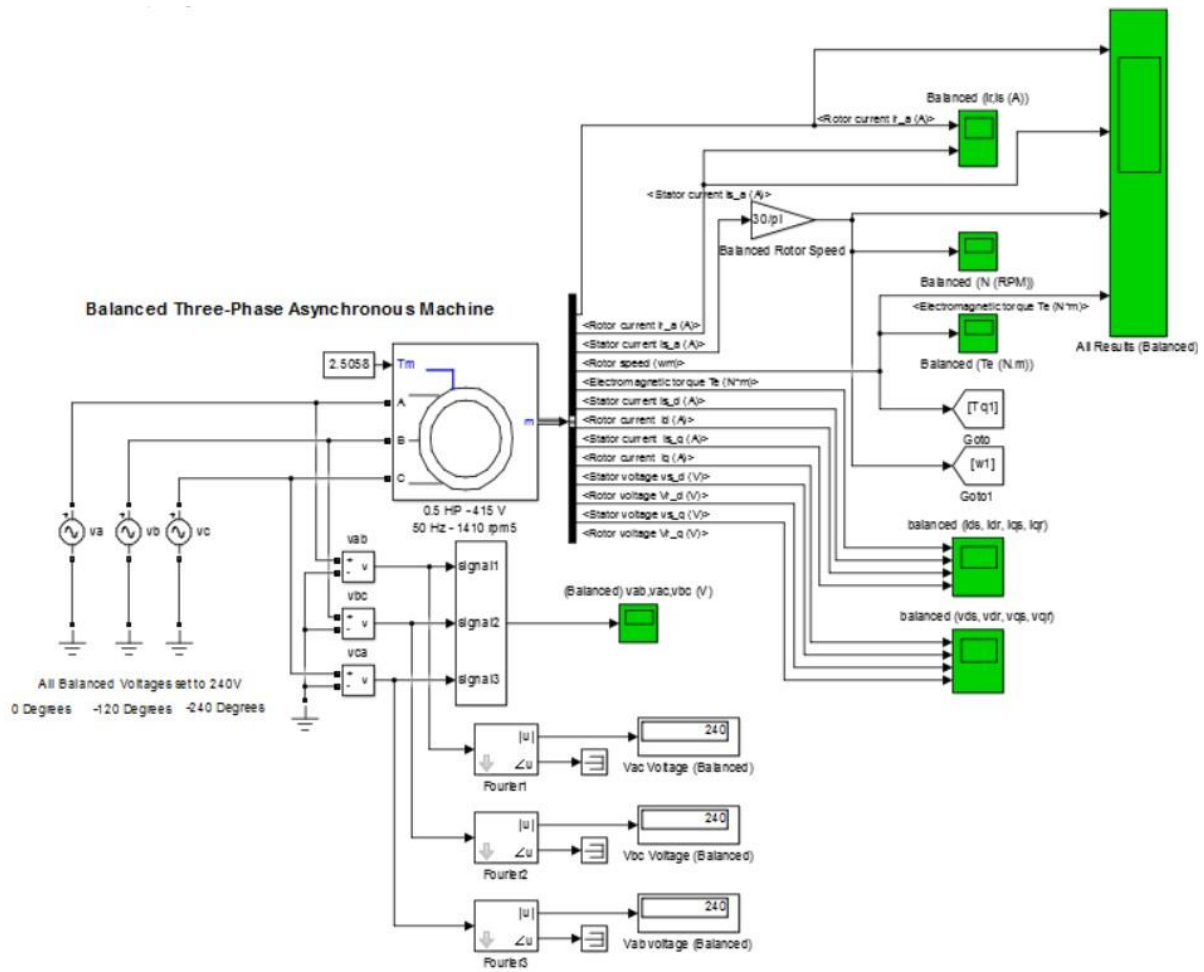
Figure 21 : Model of the Asynchronous machine with the input-out using Simulink

The unbalanced voltage situations in Table 5 were represented in the induction motor sub-systems in the Simulink environment. The impacts of various experimental circumstances on each individual motor output variable were discussed.

a. Effect on rotor current

Figure 22 depicts the impact of various imbalanced circumstances on rotor current. These are rotor current transient reactions. The plot demonstrates that after an initial magnified fluctuation of the current, it takes roughly 0.15 seconds to settle to the rated rotor current under balanced conditions. Figure 22 also shows that voltage magnitudes that are too low or too high contribute high frequency components into the steady state rotor current. A high frequency low magnitude component modulates the rotor current. Any change in the phase angle of the supply voltage, whether positive or negative, modulates the rotor current with

high frequency and magnitude components. As a result, variations in both magnitude and phase angles produce a rotor current dominated by the influence of phase angle changes. These are rotor current harmonics with high frequencies that contribute to rotor losses and heating. When a phase is lost, it causes a huge unstable high-frequency rotor current, which causes pulsing torque as seen in Figure 26 and increasing rotor speed as shown in Figure 25. Surprisingly, increasing the magnitude or phase angle resulted in a faster steady state rotor current, which is reached in 0.1 seconds.
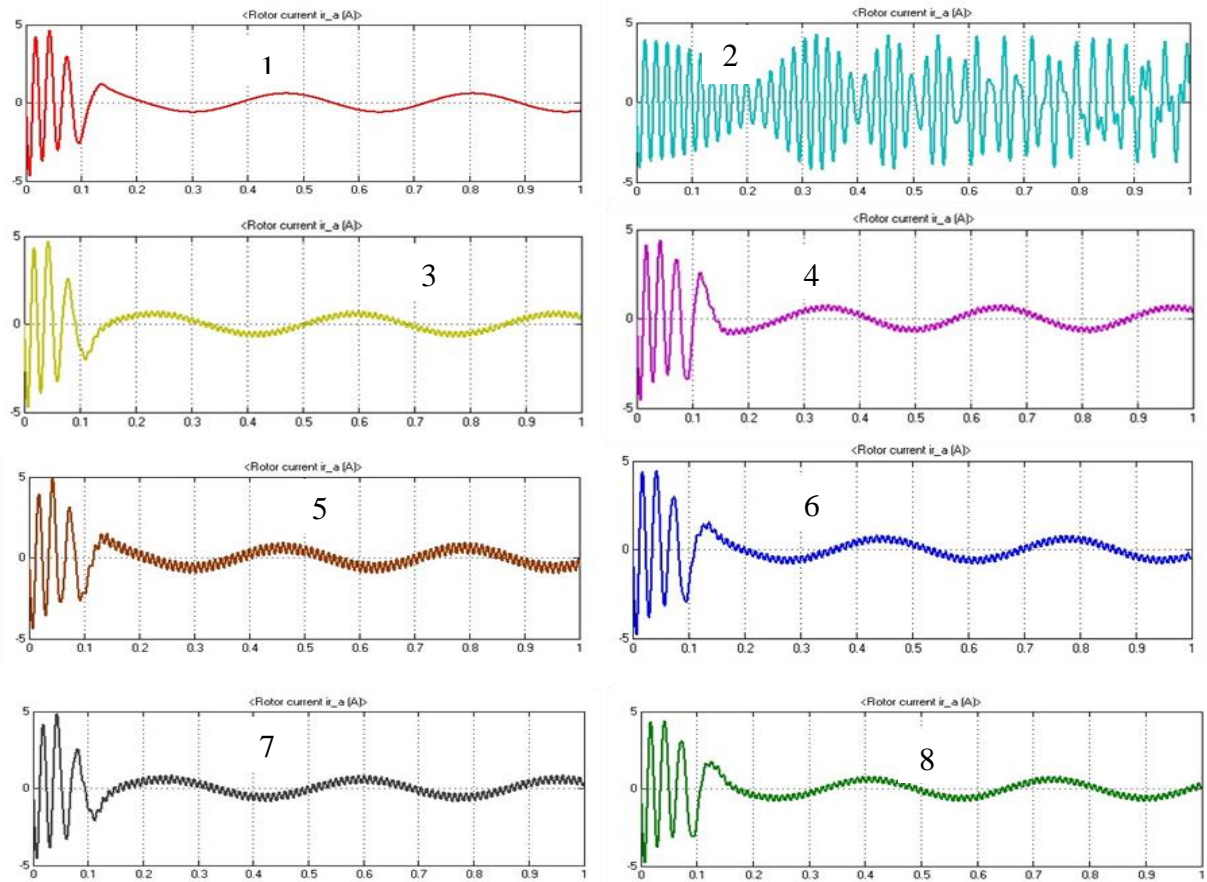
Figure 22 : Effect of different voltages imbalances on rotor current (Ir) vs. time (s)

Legends:
- 1- the balanced condition
- 2 -loss of a phase
- 3- magnitude increase
- 4- magnitude decrease
- 5- phase increase
- 6- phase decrease
- 7- increase in both magnitude and phase
- 8 -decrease in both magnitude and phase

b. Effect on stator current

Stator current, unlike rotor current, is somewhat reduced under balanced situations at greater voltage magnitude and phase angle conditions, as seen in Figure 23. A drop in voltage magnitude, on the other hand, marginally increases the steady-state stator current. As the phase angle is reduced, the stator current nearly doubles when compared to the balanced situation. A phase loss magnifies the stator current several times, implying that there is a reciprocal link between the stator current and the amplitude and phase angle of the supply voltage. This is due to the fact that at low voltage magnitudes, the stator draws greater current to maintain the input power constant.
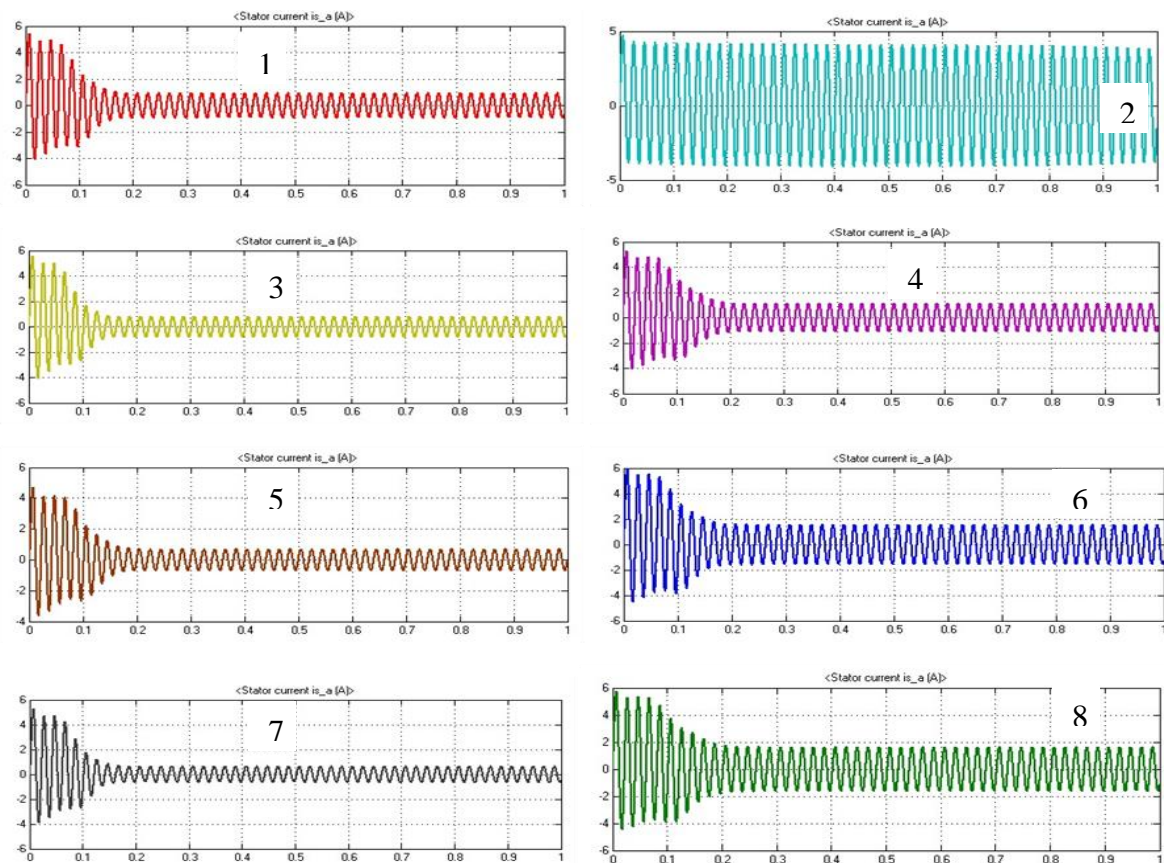
Figure 23 : Effect of different voltages imbalances on stator current (Ir) vs. time (s)

Legends:

- 1- balanced condition
- 2 -loss of a phase
- 3- magnitude increase
- 4- magnitude decrease
- 5- phase increase

- 6- phase decrease
- 7- increase in both magnitude and phase
- 8 -decrease in both magnitude and phase

c. Effect on rotor speed

Figure 24 depicts the impact of various imbalanced circumstances on rotor speed. The rotor rotates at the rated speed of 1410.8883 rpm under balanced circumstances, and steady-state is reached in 0.17 seconds. An increase in voltage gradually increases rotor speed, which achieves a steady state in 0.15 seconds. A reduction in the magnitude of the voltage or any change in the phase angle, on the other hand, leads in a minor decrease in the rotor speed. The lowest steady-state rotor speed is obtained by decreasing both the voltage magnitude and the phase angle. As seen in Fig. 24, losing a phase accelerates the rotor speed.
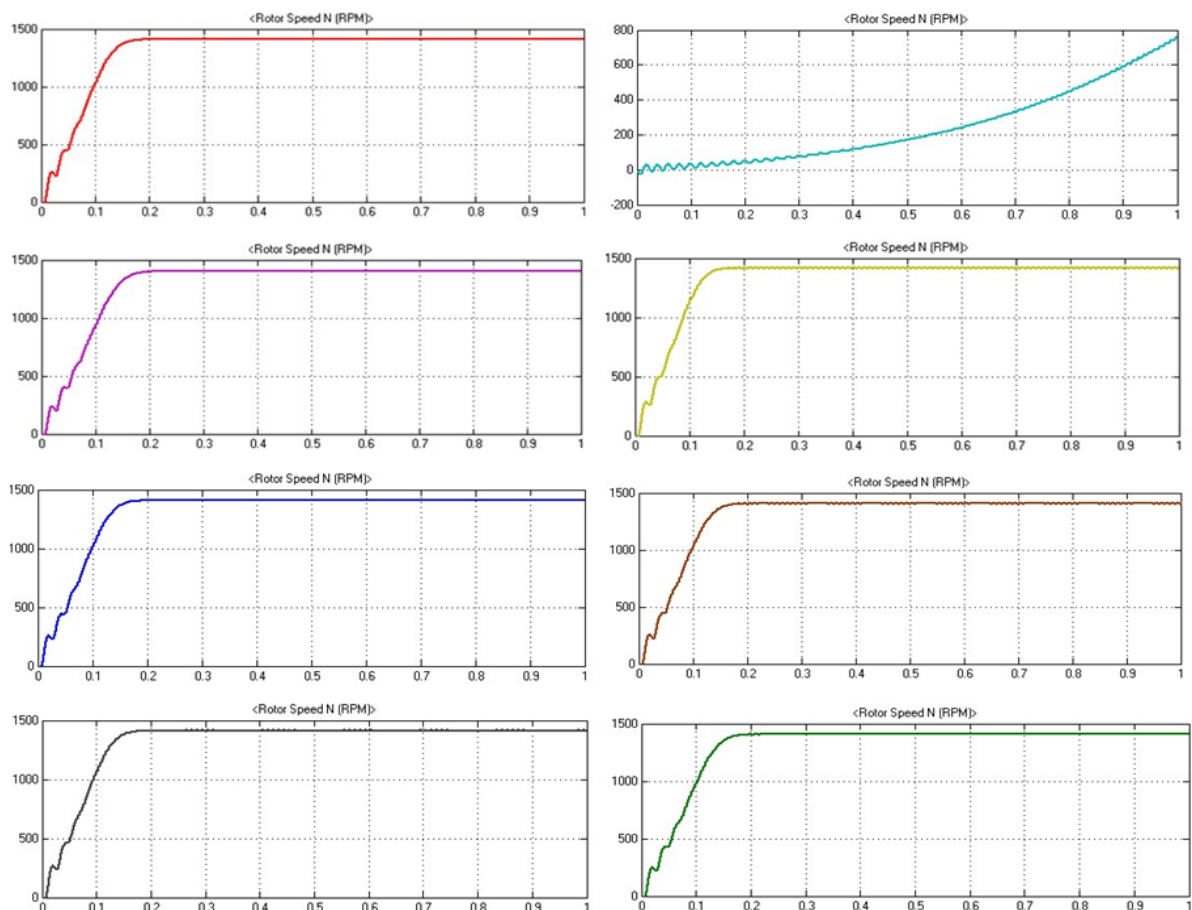

Figure 24 : Effect of different voltage imbalances on rotor speed (N) vs. time (s)

Table 6 : Rotor speed at different conditions

Experimental Conditions	Speed (RPM)
Balanced	1410.88
Magnitude Decrease	1402-1405.6
Magnitude Increase	1414.9-1416
Phase Decrease	1407.8-1413
Phase Increase	1404.9-1413
Magnitude and Phase decrease	1400-1406
Magnitude and Phase increase	1412.5-1418.5
Phase Loss	Does not reach a steady-state

Figure 25 depicts a graphic comparing steady-state and transient rotor speeds under various testing settings. As demonstrated in Figure 25, when the magnitude and/or phase angle of the voltage are lowered, the rotor speed falls below that of balanced circumstances (a). Figure 25 (b) demonstrates that increasing the voltage magnitude improves the steady-state speed, whereas increasing the voltage phase angle reduces the speed. When the magnitude and phase angle of the voltage are both raised, the steady-state speed is increased more than in balanced conditions. This enhanced steady-state speed, however, is slower than the speed recorded during overvoltage circumstances.
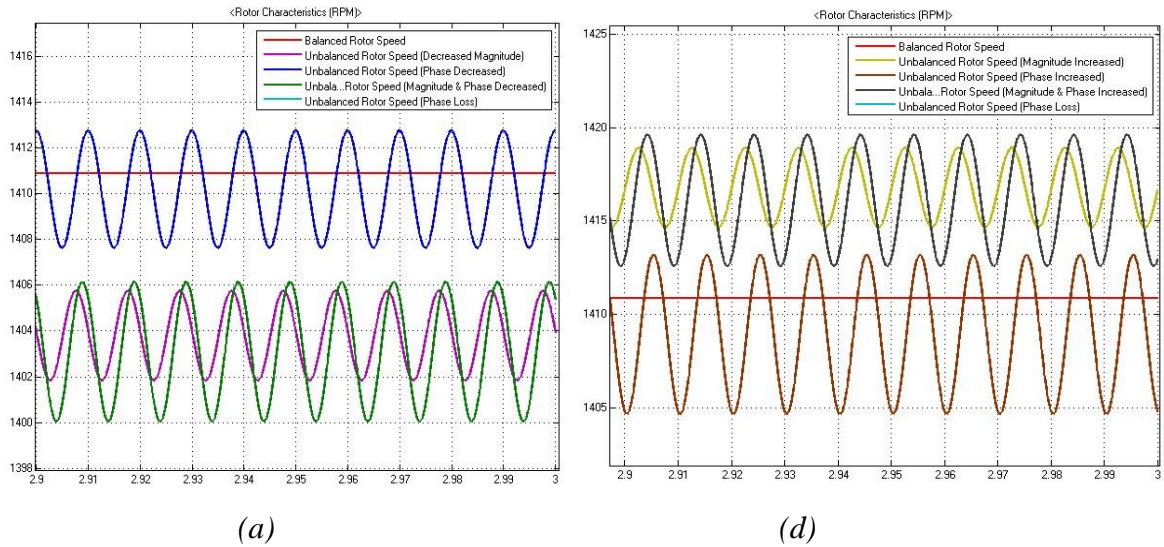

(a)   *(b)*
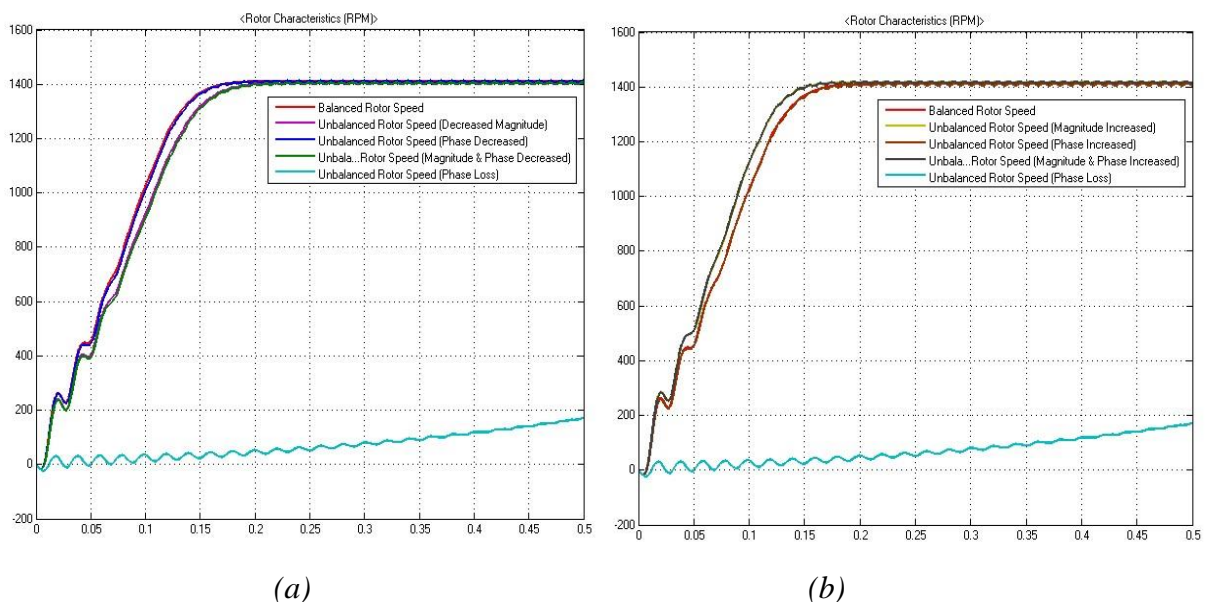
Figure 25 : Rotor Speed characteristics and Steady-state

Legends:

(a) decreased imbalances

(b) increased imbalances

(c) decreased unbalances

(d) increased unbalanced conditions

d. Effect on electromagnetic torque

Under balanced voltage settings, the torque approaches a steady-state value of 2.505 Nm after an initial transient reaction, as seen in Figure 26. However, under all unbalanced voltage settings, the torque does not remain constant at a steady state but rather oscillates. The torque oscillates at roughly 2 Nm at over and under voltage magnitude. When the phase angle changes (rises or decreases), the amplitude of the oscillation increases multiple times. When the amplitude and phase of the supply voltage are both increased, the oscillation becomes much more pronounced. However, a drop in both magnitude and phase angle results in the same torque transient as a change in phase angle. Notably, the loss of a phase causes unstable oscillations in torque, which, unlike other unbalanced voltage circumstances, never approaches a steady state.
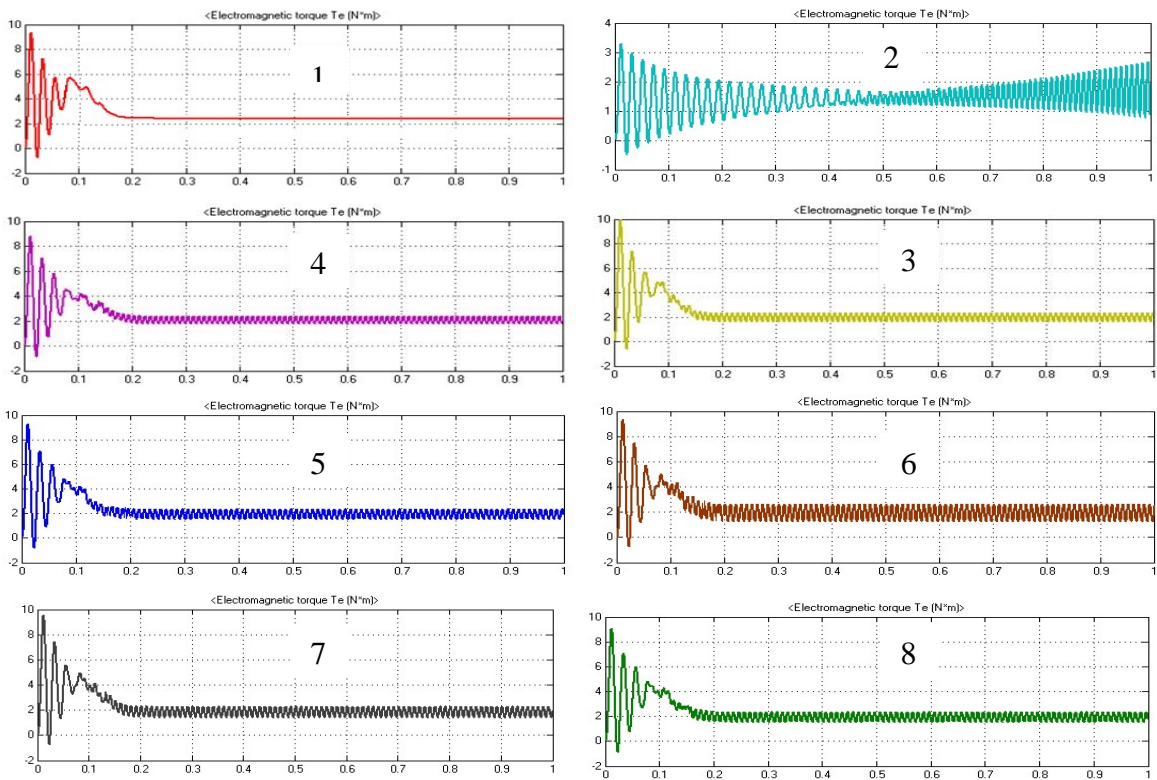
Figure 26 : Effect of different voltages imbalances on electromagnetic torque (T) vs. time (s)

Legends:

- 1- the balanced condition
- 2 -loss of a phase
- 3- magnitude increase
- 4- magnitude decrease
- 5- phase increase
- 6- phase decrease
- 7- increase in both magnitude and phase
- 8 -decrease in both magnitude and phase
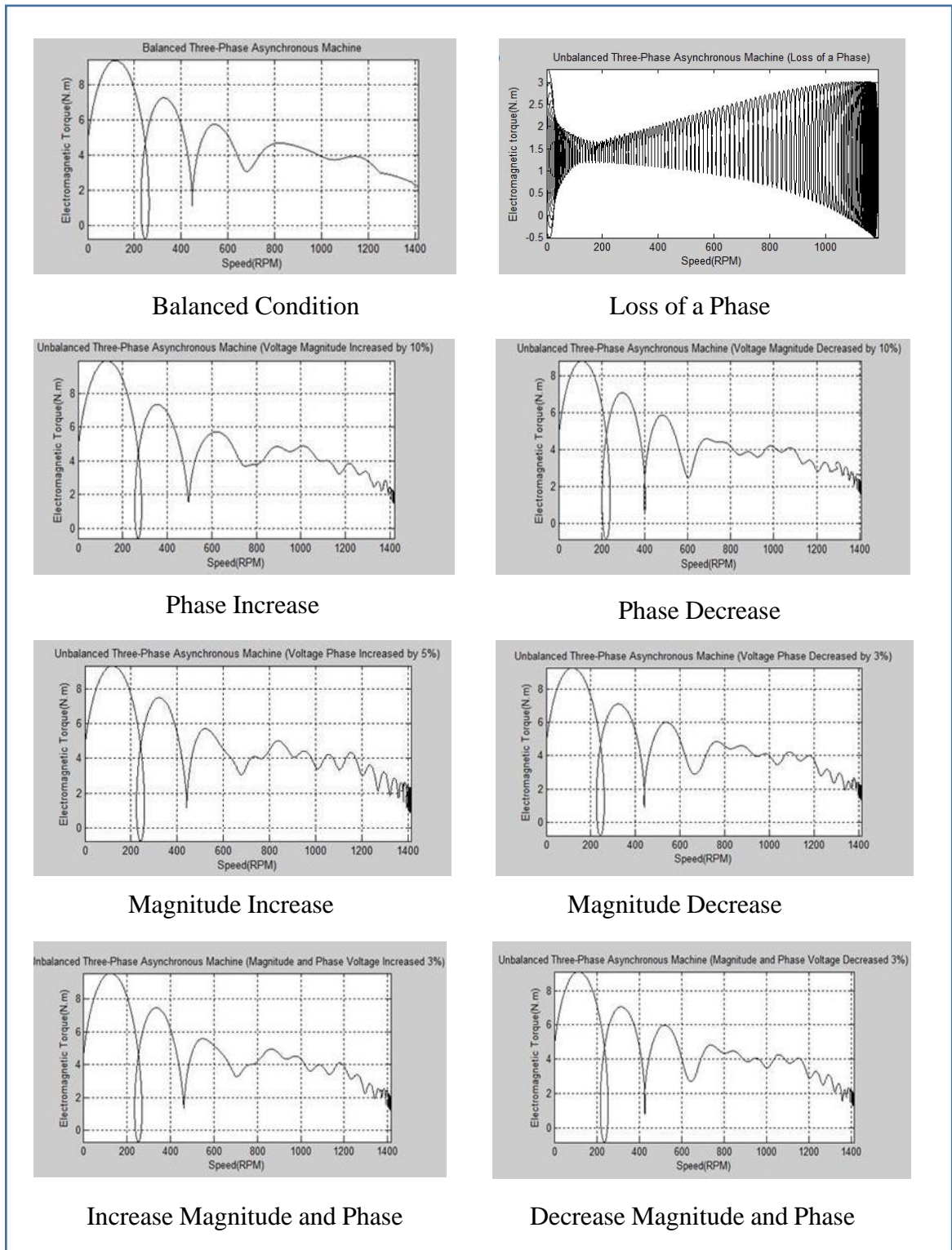
Figure 27 : Effect of different voltages imbalances on torque-speed characteristics of the induction motor

Figures 22-23 show that the stator and rotor start up currents are many times more than the rated current, as predicted. Because there is always friction in the motor's bearings, once the rotor reached its rated speed, it oscillated around it. This friction prevents the motor from

reaching synchronous speed. Figure 27 illustrates that the rotor accelerates to its rated velocity without overshooting, as predicted for high-efficiency motors.

This sort of motor offers a strong starting torque, according to the Toshiba motor catalog. Figure 27 (balanced conditions) depicts the significant electromagnetic torque generated by the motor during its initial start-up and as it accelerates to its rated speed. To be in balance with the load torque, the torque settles down to virtually a constant magnitude. Figure 27 shows that changing the phase angle causes greater oscillations in the torque-speed characteristics than changing the voltage magnitude alone.

An increase in the magnitude of the voltage accentuates the torque oscillations compared to a reduction in magnitude. In the event of a phase failure, the remaining phases will attempt to compensate for the load, resulting in unstable oscillations that get increasingly rapid with time, leading the motor to overload.

e. Effect on derating factor

Figure 28 depicts the derating curves under various imbalanced situations. As previously stated, an unbalanced voltage phase angle has a more severe effect than an imbalanced voltage magnitude. As illustrated in Fig. 28, a 15% voltage imbalance factor is required to reduce the derating factor to zero for voltage magnitude (a). In contrast, as illustrated in Fig. 28, a 5% voltage imbalance factor results in a 0% derating factor for phase angle (b).
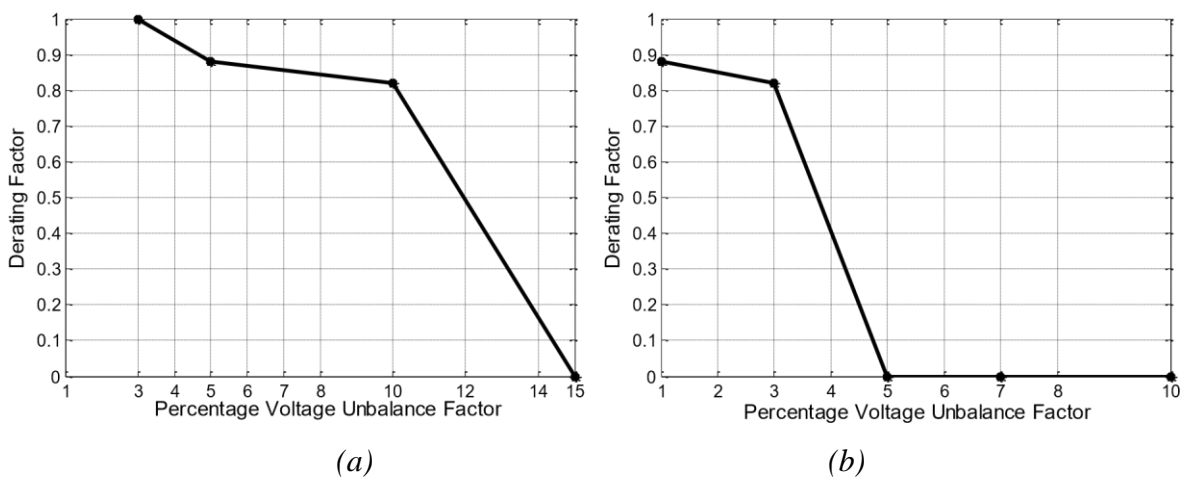

(a)   *(b)*

Figure 28 : Derating curves

(a) for increased and decreased voltage magnitude cases

(b) for increased and decreased voltage phase angles- decreased under-voltage

magnitude and phase.

Chapter 5 : Discussions

The observations depicted in the result sections require more explanation in order to determine the sources of these outcomes. Understanding the origin and impact of a particular observation will lead to a viable solution or protection strategy for loss, damage, or other negative outcomes. The discussion in the findings section focused on the impact of various imbalanced circumstances on each electrical or mechanical variable of the motor. These findings are summarized here to show the general cause and effect of the various unbalanced voltage scenarios.

Table 7 summarizes all of the charts in Figures 22-25 to make it easier to compare the impact of different unbalanced voltage circumstances on the motor variables.

Table 7 : Mechanical and Electrical variables under various unbalanced voltage circumstances. The rated values are used to compare high and low phrases

	Stator Current Magnitude (from Figure 23)	Rotor Current Ripples (from Figure 22)	Steady State Torque (Nm) (Settling time) (from Figure 26)	Average Speed (from Table 6)
Balanced	Rated	No Ripple	(0.17 s)	Rated
Magnitude Increase	Low	Lowest	(0.15 s)	Highest
Magnitude Decrease	High	Lowest	(0.2 s)	Below Rated
Phase Increase	Low	High	(0.18 s)	Below Rated
Phase Decrease	Highest	High	(0.18 s)	Below Rated
Magnitude and Phase Increase	Lowest	Highest	(0.15 s)	Close to Rated
Magnitude and Phase Decrease	Highest	High	(0.2 s)	Low
Phase Loss	Unstable	Unstable	Unstable	Lowest

Overvoltage (Magnitude Increase) has resulted in low stator current, lowest ripple, and maximum average speed. Low currents cause lesser copper losses, resulting in higher efficiency than in other imbalanced scenarios. This appears to be the finest of all potential imbalanced circumstances. However, speeds over the stated capacity may put excessive mechanical strains on the physical qualities of the motor. This is consistent with *Lee's*

findings, who discovered a better efficiency in overvoltage circumstances than in other unbalanced voltage scenarios [6]. Lee's research also revealed that when the voltage is low, the motor consumes substantially more electricity than when it is high.

Voltage phase angle variations have the greatest impact on rotor current ripples. All variations produce much greater rotor current ripples than those subjected to voltage magnitude variation. Imbalances in voltage phase angles also affect the mechanical angle of rotation, resulting in high-frequency ripples in the opposing torque created by rotor current. In general, a decrease in voltage magnitude slows the torque's settling period. A decrease in voltage magnitude induces a rise in stator current to maintain input power, delaying steady-state torque development.

The currents generated by the positive and negative sequences produce opposing rotating magnetic fields, resulting in ripples in electromagnetic torque and velocity variations. *Mirabbasi et al.* [7] also detected torque oscillations caused by imbalanced voltages, as seen in our investigation. Such oscillations generate noise, vibration, and mechanical strains, which cause machine wear and aging. Because of the voltage imbalance, the torque-speed characteristics modify the so-called values of pull-up and breakdown torque. Unbalanced voltages, in general, generate negative sequence currents that serve no function other than to contribute to power loss and temperature rise. In imbalanced situations, a decline in power factor reflects a shift in actual and reactive power consumption. Because of the imbalanced voltage, the negative sequence components contribute to excessive heat, which elevates the motor temperature and may damage the insulation. A substantial imbalance may potentially result in the motor's destruction.

The loss of a phase is the most severe imbalanced state. In comparison to any of the 15% decline situations, this scenario corresponds to a 100% fall in voltage magnitude and angle. As the motor seeks to supply its full rated power, the loss in one phase places an enormous demand on the other two. Under such conditions, all variables, from stator and rotor currents to speed and torque output, become unstable. If no precautions are taken, the motor may fail in a short period of time.

Chapter 6 : Conclusion

To understand the impacts of various unbalanced voltage circumstances, a detailed investigation of motor function was performed. The motor parameters were assessed for use in subsequent simulations that resulted in graphical displays of motor activity. Any three-phase induction motor may be built and tested for optimal functioning using this approach, either before or after construction. The modeling of motor characteristics under various voltage situations, including displays of torque-speed characteristics, line currents, and rotor speeds, may be immensely valuable in anticipating probable problems or motor design errors. Prior to manufacture, the Simulink-based MATLAB toolbox provides an ideal platform for designing and testing motor operations under various input power, faults, and/or severe unfavorable circumstances.

The behavior of a three-phase induction motor may be examined in similar ways by employing various protective methods aimed at mitigating the negative consequences of unbalanced voltages. Such research will aid in the development and optimization of protective measures or gadgets. Automatic or adaptive control systems, microcontroller-based switches, and sensor-based filters and compensators are examples of such protective methods. It is not always advisable to trip or shut down the equipment in the event of an imbalanced voltage occurrence. It is not always advisable to trip or shut down the equipment in the event of an imbalanced voltage occurrence. To maintain continuous or smooth operations in industrial applications, standby preventive mechanisms should function automatically to compensate for the detrimental consequences of negative sequence components. As a result, for a complex and robust motor design, real-time acquisition and analysis of torque-speed characteristics, currents, and torques are required. A sample motor unit test comparable to the one used in this study can be modified for larger-scale motor design and manufacturing. It would be beneficial to examine the operations and features of heavy industrial three-phase induction motors using comparable theories, especially when they are utilized for heavy-duty or important industrial activities. It is also critical to comprehend the impact of drive end load variations when combined with unbalanced voltage circumstances. This research concentrated on the influence of input power quality on motor performance, but output mechanical power needs may have distinct transitory consequences. In overload circumstances, sudden changes in load or under load investigation and modeling of these motor variables may also produce intriguing results.

References

[1]   W. L. Kenly and B. K. Bose, "Triac Speed Control of Three-Phase Induction Motor with Phase-Locked Loop Regulation," Industry Applications, IEEE Transactions on, vol. IA-12, no. 5, pp. 492–498, 1976.

[2]   "Three-phase asynchronous motors: Generalities and ABB proposals for the coordination of protective devices," ABB, Jun. 2008.

[3]   A. von Jouanne and B. Banerjee, "Assessment of voltage unbalance," Power Delivery, IEEE Transactions on, vol. 16, no. 4, pp. 782–790, Oct. 2001.

[4]   P. Pillay and M. Manyage, "Loss of Life in Induction Machines Operating With Unbalanced Supplies," Energy Conversion, IEEE Transactions on, vol. 21, no. 4, pp. 813–822, Dec. 2006.

[5]   P. Gnacinski, "Windings Temperature and Loss of Life of an Induction Machine Under Voltage Unbalance Combined With Over- or Undervoltages," Energy Conversion, IEEE Transactions on, vol. 23, no. 2, pp. 363–371, Jun. 2008.

[6]   C.-Y. Lee, "Effects of unbalanced voltage on the operation performance of a threephase induction motor," Energy Conversion, IEEE Transactions on, vol. 14, no. 2, pp. 202–208, Jun. 1999.

[7]   D. Mirabbasi, G. Seifossadat, and M. Heidari, "Effect of unbalanced voltage on operation of induction motors and its detection," in Electrical and Electronics Engineering, 2009. ELECO 2009. International Conference on, 2009, pp. I–189–I–192.

[8]   U. Jayatunga, S. Perera, and P. Ciufo, "Impact of mains connected three-phase induction motor loading levels on network voltage unbalance attenuation," in Power System Technology (POWERCON), 2012 IEEE International Conference on, 2012, pp. 1–6.

[9]   C. T. Raj, P. Agarwal, and S. P. Srivastava, "Performance Analysis of a Three-Phase Squirrel-Cage Induction Motor under Unbalanced Sinusoidal and Balanced NonSinusoidal Supply Voltages," in Power Electronics, Drives and Energy Systems, 2006. PEDES '06. International Conference on, 2006, pp. 1–4.

[10]   J. E. Williams, "Operation of 3-Phase Induction Motors on Unbalanced Voltages [includes discussion]," Power Apparatus and Systems, Part III. Transactions of the American Institute of Electrical Engineers, vol. 73, no. 1, Jan. 1954.

[11]   B. N. Gafford, W. C. Duesterhoeft, and C. C. Mosher, "Heating of Induction Motors on Unbalanced Voltages," Power Apparatus and Systems, Part III. Transactions of the American Institute of Electrical Engineers, vol. 78, no. 3, pp. 282–286, Apr. 1959.

[12]   "Energy matters industrial technology program: The effects of unbalanced voltage on the life and efficiency of three-phase electric motors," US Department of Energy and Renewable energy, Mar. 2005.

[13]   L. Guasch-Pesquer, L. Youb, F. Gonzalez-Molina, and E.-R. Zeppa-Durigutti, "Effects of voltage unbalance on torque and current of the induction motors," in Optimization of Electrical and Electronic Equipment (OPTIM), 2012 13th International Conference on, 2012, pp. 647–652.

[14]   R. F. Woll, "Effect of Unbalanced Voltage on the Operation of Polyphase Induction Motors," Industry Applications, IEEE Transactions on, vol. IA-11, no. 1, pp. 38–42, Jan. 1975.

[15]   E. Quispe, P. Viego, and J. Cogollos, "Statistical equations to evaluate the effects of voltage unbalance on the efficiency and power factor of a three-phase induction motors," WSEAS Trans. Circuits Syst., vol. 4, pp. 234–239, 2005.

[16]   *"Power quality solutions for industrial customers," California energy commission, Aug. 2000.*

[17]   *S. B. Singh, A. K. Singh, and P. Thakur, "Assessment of induction motor performance under voltage unbalance condition," in Harmonics and Quality of Power (ICHQP), 2012 IEEE 15th International Conference on, 2012, pp. 256–261.*

[18]   *R. Automation, "Application basics of operation of three-phase induction motors," WPmotors, 1996.*

[19]   *J. R. Jenneson, Electrical Principles For The Electrical Trades. New South Wales, Australia: McGraw-Hill Book Company, 1985.*

[20]   *S. J. Chapman, Electric Machinery Fundamentals, 4 th. New York: The McGraw-Hill Companies, 2005.*

[21]   *R. M. Hamouda, A. J. Alohah, and M. A. Badr, "Electromechanical transient of series connected three phase slip ring induction motors," in Power Engineering Society Winter Meeting, 2000. IEEE, 2000, vol. 1, pp. 260–263 vol.1.*

STUDY PERFORMANCE OF A THREE-PHASE INDUCTION MOTOR UNDER UNBALANCED CONDITIONS

Approved by:

Dr. MD. FOKHRUL ISLAM

Supervisor and Professor,
Department of Electrical and Electronic Engineering,
Islamic University of Technology (IUT),
Board Bazar, Gazipur-1704.

Date: 12/05/2022

Declaration of Authorship

This is the attestation of the work done in the thesis paper by the students Ibrahim Abdou Ibrahima, Abdurrahman Omar Abdou, and Mohaman Djibrilla under the supervision of Dr. Md. Fokhrul Islam, Professor of Department of Electrical and Electronic Engineering (EEE), Islamic University of Technology (IUT), a subsidiary organ of the Organization of Islamic Cooperation (OIC).

Authors

IBRAHIM ABDOU IBRAHIMA
ID-170021172

ABDOURRAHMAN OMAR ABDOU
ID-170021173

MOHAMAN DJIBRILLA
ID-170021180

I